Revision 1

Compressional and shear wave velocities for polycrystalline bcc-Fe up to 6.3 GPa and 800 K

Yuki Shibazaki [1, 2], Keisuke Nishida [3], Yuji Higo [4], Mako Igarashi [2], Masaki Tahara [2], Tatsuya Sakamaki [2], Hidenori Terasaki [5], Yuta Shimoyama [5], Souma Kuwabara [5], Yusaku Takubo [5], Eiji Ohtani [2]

[1]Frontier Research Institute for Interdisciplinary Sciences, Tohoku University, 6-3 Aoba, Aramaki, Aoba-ku, Sendai 980-8578, Japan.

[2]Department of Earth and Planetary Material Sciences, Tohoku University, 6-3 Aoba, Aramaki, Aoba-ku, Sendai 980-8578, Japan.

[3]Department of Earth and Planetary Science, University of Tokyo, Hongo 7-3-1, Bunkyo-ku, Tokyo 113-0033, Japan.

[4]Japan Synchrotron Radiation Research Institute, 1-1-1 Kouto, Sayo 679-5198, Japan.

[5]Department of Earth and Space Science, Osaka University, 1-1 Machikaneyama-cho,

Toyonaka, Osaka 560-0043, Japan.

Corresponding author: Yuki Shibazaki

Frontier Research Institute for Interdisciplinary Sciences, Tohoku University, 6-3 Aoba, Aramaki, Aoba-ku, Sendai 980-8578, Japan.

E-mail: yshibazaki@m.tohoku.ac.jp

Tel: +81-22-795-6687

Keywords: bcc-Fe, high pressure, planetary core, sound velocity, ultrasonic method

Running title: Sound velocities for bcc-Fe

Abstract

The cores of the Earth and other differentiated bodies are believed to comprise iron and various amounts of light elements. Measuring the densities and sound velocities of iron and its alloys at high pressure and high temperature is crucial for understanding the structure and composition of these cores. In this study, the sound velocities (V_P and V_S) and density measurements of body-centered cubic (*bcc*)-Fe were determined experimentally up to 6.3

GPa and 800 K using ultrasonic and X-ray diffraction methods. Based on the measured V_P, V_S, and density, we obtained the following parameters regarding the adiabatic bulk K_S and shear G moduli of *bcc*-Fe: K_{S0} = 163.2(15) GPa, $\partial K_S/\partial P$ = 6.75(33), $\partial K_S/\partial T$ = –0.038(3) GPa/K, G_0 = 81.4(6) GPa, $\partial G/\partial P$ = 1.66(14), and $\partial G/\partial T$ = –0.029(1) GPa/K. Moreover, we observed that the sound velocity–density relationship for *bcc*-Fe depended on temperature in the pressure and temperature ranges analyzed in this study and the effect of temperature on V_S was stronger than that on V_P at a constant density, e.g., 6.0% and 2.7% depression for V_S and V_P, respectively, from 300 K to 800 K at 8000 kg/m^3. Furthermore, the effects of temperature on both V_P and V_S at a constant density were much greater for *bcc*-Fe than for *ε*-FeSi (cubic B20 structure), according to previously obtained measurements, which may be attributable to differences in the degree of thermal pressure. These results suggest that the effects of temperature on the sound velocity–density relationship for Fe alloys strongly depend on their crystal structures and light element contents in the range of pressure and temperature studied.

Introduction

Observations of seismic wave propagation and normal mode oscillation are the most powerful probes for examining the Earth's interior, allowing us to obtain physical information on the Earth's interior such as distributions of densities and sound velocities (both compressional (V_P) and shear (V_S) wave velocities) (e.g., Preliminary Reference Earth Model (PREM), proposed by Dziewonski and Anderson (1981)). According to observation-based geophysical data and laboratory-based studies, the Earth's core is considered to comprise metallic iron (Fe) with various amounts of light elements, such as hydrogen (H), carbon (C), oxygen (O), silicon (Si), and sulfur (S) (e.g., Birch 1952; Poirier 1994). Thus, iron alloyed with light elements is widely accepted as a basis for the chemical models of other planetary cores (e.g., Zharkov et al. 2009; Dumberry and Rivoldini 2015).

To constrain the species of major light elements and their abundances in the core, many studies have investigated the density and sound velocity of Fe as well as its alloys with light elements at the high pressures and high temperatures characteristic of interior planetary conditions (see the review by Li and Fei 2014). At high pressure and temperature, sound velocities have been measured mainly using shock compression (e.g., Brown and McQueen 1986), high-energy resolution inelastic X-ray scattering (IXS) (e.g., Fiquet et al.

2001; Badro et al. 2007), and nuclear resonant inelastic X-ray scattering (NRIXS) (e.g., Mao et al. 2001; Lin et al. 2003). Most recently, measurements by picosecond acoustics have been reported (Decremps et al. 2014). However, to estimate V_S (and also V_P in the case of NRIXS), those measurements require other physical quantities (e.g., density and bulk modulus) that must be obtained in separate experiments. That is, V_S (and V_P of NRIXS) must be obtained indirectly, and thus the accuracy of the estimated value depends on the uncertainties of these physical quantities as well as the velocity measurement itself. Therefore, most core compositional models have been developed using only V_P data, although the proposed physical models for the Earth's interior (e.g., PREM) provide us with both V_P and V_S for the solid inner core. To constrain the abundances of light elements in the core more tightly, direct measurements of V_S for Fe and Fe alloys and core compositional analyses using both V_P and V_S are necessary.

Analyses based on V_P have also led to another issue, i.e., disagreements in the temperature dependence of sound velocities between previous studies (see the review by Antonangeli and Ohtani (2015)). The sound velocity–density relationship has been used widely to compare experimental results with proposed physical models for the Earth's interior (e.g., Lin et al. 2004; Gao et al. 2008; Fiquet et al. 2009, Antonangeli et al. 2010;

Shibazaki et al. 2012; Murphy et al. 2013; Kamada et al. 2014). Assuming a quasi-harmonic approximation, this relationship is expected to exhibit linearity regardless of the pressure and temperature conditions, which is known as Birch's law (Birch 1961). On the other hand, when a nonharmonic temperature effect appears, the velocity–density relationship is likely to change significantly with the temperature. Recent studies have investigated the effects of temperature on the sound velocity–density relationship for Fe and Fe alloys at high pressures using the IXS (Kantor et al. 2007; Antonangeli et al. 2012; Mao et al. 2012; Ohtani et al. 2013; Liu et al. 2014; Antonangeli et al. 2015) and NRIXS (Lin et al. 2005; Gao et al. 2011) techniques, but no consensus has been reached regarding the effects of temperature. Previous ab initio molecular dynamics simulations showed that the effect of temperature on V_P is small compared with that on V_S (e.g., Vočadlo et al. 2009; Sha and Cohen 2010). Then, the experimental temperatures used in previous studies might be too low to observe clearly that on V_P. In contrast, measuring V_S is expected to facilitate clear analyses of the effects of temperature on the velocity–density relationship, even at relatively low temperatures.

In this study, as a first step toward addressing these issues (i.e., discussions on the temperature dependence of sound velocities and the core compositions using both V_P and

V_S), we directly measured both V_P and V_S and the density of body-centered cubic (*bcc*)-Fe up to 6.3 GPa and 800 K using an ultrasonic technique, X-ray radiography, and X-ray diffraction methods. The *bcc* phase is a low-pressure and -temperature phase and the most fundamental structure for Fe (e.g., Bundy 1965). Recently, Liu et al. (2014) and Antonangeli et al. (2015) obtained high-pressure and high-temperature data of V_P for *bcc*-Fe using IXS techniques, but they reported different temperature dependences for V_P, and there were no discussions on V_S. In the present study, we analyzed the effects of temperature on the sound velocity–density relationships of both V_P and V_S for *bcc*-Fe and discussed the difference in the effects of temperature between Fe and Fe compounds.

Experimental Methods

High-pressure and high-temperature ultrasonic measurements and X-ray radiography and diffraction experiments were performed simultaneously using the 1500-ton Kawai-type multianvil apparatus (SPEED-1500) with synchrotron X-ray radiation at the BL04B1 beamline of the SPring-8 facility in Japan. The experimental pressure range was

2.0 to 6.3 GPa at temperatures up to about 800 K. We used a 14/8 cell assembly (14 mm octahedron edge length and 8 mm truncated edge length of tungsten carbide cubic anvils). Figure 1a is a schematic illustration of the cell assembly used in this study. Iron powder (99.99% purity, Rare Metallic Co. Ltd.) was used as a starting material, which was sandwiched between an yttrium-stabilized zirconia (YSZ) buffer rod and backing plate (mirrored on both surfaces), and surrounded by cup-shaped hexagonal boron nitride (hBN). A powdered mixture of magnesium oxide (MgO) and hBN, placed just behind the hBN cup, was used as a pressure marker. High temperatures were generated using a cylindrical graphite heater.

The experimental temperatures and pressures were estimated simultaneously based on two equations of state, i.e., that for MgO (Tange et al. 2009) and that for hBN (Wakabayashi and Funamori 2015), as the pressure marker, as follows. Using the test assembly with a W3%Re–W25%Re thermocouple (TC) (Fig. 1b), we performed an in situ X-ray diffraction experiment and measured the transition temperature between the *bcc* and face-centered cubic (*fcc*) phases of Fe at approximately 2 GPa, thereby determining the temperature difference between the sample and TC positions in the assembly. The results showed that the TC temperature was approximately 120 K lower than the *bcc*–*fcc* transition temperature reported by Claussen (1960), whereas the temperature based on the two equations of state for the pressure marker was consistent with the reported temperature. This difference probably occurred because the TC position was off-center and away from the sample. Additional experiments were performed, in which the pressure markers were placed in both the sample and original pressure marker positions at approximately 1 GPa up to 800 K and at approximately 5.5 GPa up to 1000 K, using the cell assembly used for simultaneous sound velocity and density measurements (Fig. 1a). The differences in temperature between the two positions were less than 40 K under both pressure conditions, being less than the uncertainty in the temperature estimates. Therefore, we considered the temperatures and pressures by the two equations of state to be most appropriate as the experimental conditions in this study.

Ultrasonic V_P and V_S measurements were performed using a pulse-echo overlap technique (see Higo et al. (2009) for details of the experimental setup). Both P- and S-wave signals were generated and received by a 10° Y-cut $LiNbO_3$ transducer with a thickness of 0.05 mm and diameter of 3.2 mm. An electrical sine wave (three cycles) was generated by a waveform generator, and a series of reflected P- and S-wave signals were acquired by a digital oscilloscope at a sampling rate of 1.0×10^{10} points/s (0.1 ns at each data point). The frequencies used in this study were 57 MHz and 30 MHz for P- and S-waves, respectively, because we could obtain the reflected signals with best signal-to-noise ratio using these frequencies. The P- and S-wave travel times in the sample were estimated using the signals reflected from the buffer-rod/sample and sample/backing. The sample lengths at high pressure and high temperature were measured from an X-ray radiography image using a high-resolution CCD camera. The resolution of the optical setup was about 2 μm/pixel. Then, V_P and V_S were obtained simply by dividing the sample length by the P- and S-wave travel times, respectively, under each of the pressure and temperature conditions. In this study, the typical travel times (two way) were 240 ns for P-waves and 440 ns for S-waves, and the typical sample length was 700 μm. The sampling rate for the ultrasonic measurements (0.1 ns at each data point) and the optical resolution for X-ray radiography (about 2 μm/pixel) were sufficient to determine V_P and V_S precisely. The uncertainties in V_P and V_S were derived mainly from the uncertainty in the sample length determination, i.e., approximately ±1% (2σ) in this study (Table 1).

The unit-cell volumes of the sample and the pressure marker were determined based on an energy-dispersive X-ray diffraction measurement. A Ge solid-state detector was placed at a fixed angle of approximately 6° from the incident X-ray beam. The incident and receiving X-ray slit sizes were 0.1 × 0.05 mm and 2.0 × 0.2 mm, respectively. The collection time of diffraction patterns was 120 s.

First, we increased the pressure to approximately 3 GPa and the temperature to approximately 800 K to reduce the deviatoric stress imposed on the sample during compression. We then collected the ultrasonic, X-ray radiography, and X-ray diffraction data every 100–150 K while decreasing the temperature. After cooling the sample to room temperature, it was then re-pressurized and re-heated to the next target pressure and temperature conditions, and then data were again collected while decreasing temperature. We repeated this procedure at pressures up to approximately 7 GPa. All of the pressure and temperature conditions were in the stability field for the *bcc* phase (Bundy 1965).

The chemical composition of the recovered sample was analyzed using a wavelength-dispersive electron microprobe (JEOL, JXA-8800M), installed at Tohoku University, Japan, to check for contamination of the Fe sample, especially oxidization. The accelerating voltage and beam current were 15 kV and 20 nA, respectively. The beam size was 1 μm in diameter. The sample grain size was observed using a scanning electron microscope (JEOL, JSM-5410) at Tohoku University.

Results

Experimental results

The experimental conditions and results are summarized in Table 1. The chemical composition of the recovered sample (number of analyses = 21) was 99.77(51) wt% Fe and 0.22(3) wt% O, but other elements, such as Zr and Y, were not detected in the iron grains. The grain size was approximately 5 μm. Oxides such as FeO were not observed. Oxygen could increase the value of V_P for Fe and decrease its density (Badro et al. 2007), but, as described in detail in later sections, the values of V_P, V_S, density (unit-cell volume), and elastic moduli were consistent with previously reported values for *bcc*-Fe within the known margins of error. Thus, we considered the effect of 0.22(3) wt% O on these values to be negligible in this study.

Figure 2 shows the diffraction patterns obtained for the samples at ambient conditions and at the highest pressure of 6.3 GPa and 640 K. We observed the diffraction lines for *bcc*-Fe throughout the experiments, which indicated that the experimental conditions did not cross any phase boundaries (i.e., *bcc*–*fcc* or *bcc*–hexagonal close-packed (*hcp*) boundaries). Moreover, the intensity and width (full width at half maximum) of each peak were almost the same at high pressure and high temperatures as those at ambient conditions (Fig. 2). These results suggest that the deviatoric stress and preferred orientation of the sample were minimal in this study.

Examples of the P- and S-wave signals obtained at 6.3 GPa and 640 K are shown in Fig. 3a and 3b, respectively. The amplitudes of the echoes from the buffer-rod/sample and sample/backing were low compared with others, such as those from the anvil/buffer-rod and backing/hBN, due to the small difference in impedance between the sample and YSZ, but the signal-to-noise ratios were sufficient to determine the precise travel times for both P- and S-waves (Fig. 3 inserts).

Pressure and temperature dependences of the unit-cell volume and sound velocities for bcc-Fe

Figure 4 shows the unit-cell volumes obtained in the present study and the compressional curves for *bcc*-Fe reported by Zhang and Guyot (1999) and volume data from previous IXS studies (Liu et al. 2014; Antonangeli et al. 2015). The unit-cell volumes around 6 GPa in the present study were slightly lower than the compressional curves, but they were consistent within errors for the pressure and temperature. The volumes obtained from IXS studies by X-ray diffraction method (Liu et al. 2014; Antonangeli et al. 2015) were higher than the compressional curve (Zhang and Guyot 1999). Those inconsistencies may have been due to the use of different pressure scales, i.e., Liu et al. (2014) used a Au pressure scale (Fei et al. 2007), whereas Antonangeli et al. (2015) employed a ruby fluorescence method at ambient temperature as well as the *bcc*-Fe equation of state, which they derived fitting the volume data from Huang et al. (1987) with a third-order Birch–Murnaghan equation of state, at high temperature, although there might also be some issues with the volume measurements and temperature determinations by Liu et al. (2014) and Antonangeli et al. (2015). Figures 5a and 5b show the pressure dependences of V_P and V_S, respectively, for *bcc*-Fe in the present study, together with picosecond acoustics (Decremps et al. 2014), IXS studies (Liu et al. 2014; Antonangeli et al. 2015), and an ambient-pressure study, where the sound velocities were estimated with the single-crystal elastic constants given by Dever (1972) using the Voigt–Reuss–Hill average. The pressure values of the IXS studies were re-estimated based on the *bcc*-Fe equation of state described by Zhang and Guyot (1999). Those of picosecond acoustics were measured using ruby fluorescence (Decremps et al. 2014). The values obtained for V_P and V_S in the present study increased with pressure and decreased with increasing temperature. These trends agree with previous studies (Dever 1972; Decremps et al. 2014; Liu et al. 2014; Antonangeli et al. 2015), but the absolute values of V_P obtained in the present study were different from the picosecond acoustics (Decremps et al. 2014) and IXS data (Liu et al. 2014; Antonangeli et al. 2015) (Fig. 5a). We discuss the differences in the values for V_P in the present study and previous studies in detail in the "Comparison with previous high-pressure results" section in the Discussions.

Elastic moduli for bcc-Fe

We calculated the adiabatic bulk (K_S) and shear (G) moduli using the following relationships:

$$K_S = \left(V_P^2 - \frac{4}{3}V_S^2\right)\rho, \tag{1}$$

$$G = V_S^2\rho, \tag{2}$$

where ρ is the density. The calculated values of K_S and G are listed in Table 1 and shown in Fig. 6. They seem to increase monotonically with pressure and decrease with increasing temperature in the pressure and temperature ranges considered in this study. Assuming linear pressure and temperature dependences for K_S and G, we fitted K_S and G in this study using the following equation:

$$M = M_0 + \frac{\partial M}{\partial P}(P - P_0) + \frac{\partial M}{\partial T}(T - T_0), \qquad (3)$$

where M and M_0 denote K_S or G in high-pressure and high-temperature conditions and in ambient conditions, respectively. $\partial M/\partial P$ and $\partial M/\partial T$ are the pressure and temperature derivatives, respectively. P is the pressure in gigapascal and P_0 = 0 GPa. T is the temperature in kelvin and T_0 = 300 K. We obtained K_{S0} = 163.2(15) GPa, $\partial K_S/\partial P$ = 6.75(33), $\partial K_S/\partial T$ = –0.038(3) GPa/K, G_0 = 81.4(6) GPa, $\partial G/\partial P$ = 1.66(14), and $\partial G/\partial T$ = –0.029(1) GPa/K (Table 2). The fitting lines at 300 K, 400 K, 500 K, 600 K, and 700 K are shown in Fig. 6.

We can convert an adiabatic bulk modulus K_S to an isothermal bulk modulus K_T using the thermodynamic relationship:

$$K_S = (1 + \alpha\gamma T)K_T, \qquad (4)$$

where α and γ are a thermal expansion coefficient and a thermodynamic Grüneisen parameter, respectively. We estimated K_T (Table 1) by assuming that these parameters were constant ($\alpha = 4.51 \times 10^{-5}$ K^{-1} from Zhang and Guyot (1999) and γ = 1.65 from Quareni and Mulargia (1988)). Using the estimated values of K_T and equation (3), we obtained K_{T0} = 159.9(15) GPa, $\partial K_T/\partial P$ = 6.52(32), and $\partial K_T/\partial T$ = –0.049(3) GPa/K. All of the estimated elastic moduli and the previously obtained values for single-crystal and polycrystalline *bcc*-Fe are summarized in Table 2. The elastic moduli values obtained in the present study agreed with the previously reported values, except for the pressure derivatives ($\partial K_S/\partial P$, $\partial K_T/\partial P$, and $\partial G/\partial P$). However, if we assumed the same values as previous studies ($\partial K_S/\partial P$ = 6.0 (Rotter and Smith 1966), $\partial K_T/\partial P$ = 5.5 (Takahashi et al. 1968), and $\partial G/\partial P$ = 1.9 (Rotter and Smith 1966)), we could obtain similar values for K_{S0}, K_{T0}, and G_0, as well as their temperature derivatives, to those reported previously (Rotter and Smith 1966; Takahashi et al. 1968), as shown in Table 2.

Discussions

Temperature dependences of V_P, V_S, the bulk sound velocity (V_Φ), and elastic moduli (K_S and G) for bcc-Fe

The bulk sound velocity (V_Φ) is defined as follows:

$$V_\Phi = \sqrt{\frac{K_S}{\rho}}, \quad (5)$$

The values of V_Φ calculated in each of the pressure and temperature conditions are listed in

Table 1, and Fig. 7a shows the temperature dependences of V_P, V_S, and V_Φ at approximately constant pressure (2–3 GPa). In the pressure and temperature range analyzed in this study, V_Φ exhibited a relatively small temperature dependence (2.5% depression from 300 K to 700 K), whereas V_S exhibited a large dependence (6.0% depression). This smaller temperature dependence of V_Φ (=$\sqrt{K_S/\rho}$) than V_S (=$\sqrt{G/\rho}$) reflects the smaller effect of the temperature on K_S than G (Fig. 7b). The large temperature dependence of V_S for *bcc*-Fe observed in this study is the same as that for *hcp*-Fe (e.g., Vočadlo et al. 2009), while the temperature dependence of V_Φ for *bcc*-Fe is different from that for *hcp*-Fe (e.g., Vočadlo et al. 2009) and liquid Fe (Ichikawa et al. 2014), which reported that V_Φ was quite independent of temperature at approximately 300 GPa and even several thousand kelvin based on ab initio molecular dynamics simulations. This V_Φ difference between *bcc*-Fe and *hcp*-Fe (and liquid Fe) may be due to the difference of the temperature dependence of K_S. As shown in Fig. 7b, the K_S of *bcc*-Fe clearly decreased with increasing temperature (6% depression from 300 K to 700 K at 2–3 GPa). In contrast, Vočadlo et al. (2009) showed that the K_S of *hcp*-Fe exhibited only 4% depression even with increasing temperature from 0 K to 5500 K at approximately 300 GPa. Thus, the difference of the temperature dependence of V_Φ between *bcc*-Fe and *hcp*-Fe may result from a decrease in effect of the temperature on K_S with increasing pressure.

In the present study, both K_S and G decreased linearly as the temperature increased up to 700 K at approximately 2–3 GPa. These trends agreed well with previously reported results obtained at ambient pressure (Dever 1972), as shown in Fig. 7b. Dever (1972) showed that K_S and G at ambient pressure monotonically decreased with increasing temperature in the ferromagnetic region and rapidly dropped near the magnetic transition (1043 K, the Curie temperature of Fe), indicating that magnetism influences the elastic constants of *bcc*-Fe at ambient pressure. Because K_S and G at 2–3 GPa in this study exhibited the same temperature dependences as those in the ferromagnetic region at ambient pressure (Fig. 7b), the elastic moduli at 2–3 GPa might also be influenced by magnetism. In order to verify the magnetic contributions to the elastic moduli of Fe at high pressure, additional measurements of the elastic moduli and magnetism in the wide range of pressure and temperature conditions must be conducted.

Effect of temperature on the sound velocity–density relationship for bcc-Fe

Figure 8 shows the values of V_P and V_S, obtained as a function of density, together with previously reported *bcc*-Fe single-crystal data at ambient pressure (Dever 1972). Our

V_P and V_S data appeared to depend not only on density but also temperature, which clearly indicates that the temperature affected the sound velocity–density relationship for *bcc*-Fe in the pressure and temperature ranges analyzed in this study. We assumed the following linear temperature dependence for the velocity–density relationship as the first-order approximation:

$$V_{\mathrm{P,S}} = a^{\mathrm{P,S}}\rho + b^{\mathrm{P,S}}(T), \quad (6)$$

$$b^{\mathrm{P,S}}(T) = b_0^{\mathrm{P,S}} + b_1^{\mathrm{P,S}}(T - T_0), \quad (7)$$

where $a^{\mathrm{P,S}}$, $b_0^{\mathrm{P,S}}$, and $b_1^{\mathrm{P,S}}$ are constant parameters for V_P and V_S, respectively. After fitting our results with relationships (6) and (7), we obtained a^P = 1100(56), b_0^P = –2753(454), and b_1^P = –0.33(4) for V_P and a^S = 304(46), b_0^S = 831(369), and b_1^S = –0.39(3) for V_S. The calculated lines are shown in Fig. 8. The values of V_S drop more at high temperatures (b_1^S = –0.39(3)) than that of V_P (b_1^P = –0.33(4)), e.g., 6.0% and 2.7% depression for V_S and V_P, respectively, from 300 K to 800 K at 8000 kg/m^3. The effects of temperature on the sound velocity–density relationship for both V_P and V_S were consistent with the data obtained at ambient pressure (Dever 1972), although the lines for V_P extrapolated to the ambient pressure were slightly lower than the reported ambient pressure results (though the results were consistent within error).

Comparison with previous high-pressure results

We compared the results of the present study with previously reported picosecond acoustics (Decremps et al. 2014) and IXS studies (Liu et al. 2014; Antonangeli et al. 2015) using the sound velocity–density relationship because both the sound velocities and densities were measured directly, except the densities of Decremps et al. (2014) which were obtained from the equation of state of Fe. Figure 9 compares the results of this ultrasonic study and previous picosecond acoustics and IXS studies. The densities of Decremps et al. (2014) plotted in Fig. 9 were estimated based on the equation of state of *bcc*-Fe reported by Zhang and Guyot (1999). Our results at 300 K were consistent with the results of the picosecond acoustics and IXS at 300 K reported by Antonangeli et al. (2015). High temperature data of Antonangeli et al. (2015) seemed to be too scattered to define a high temperature trend, and Antonangeli et al. (2015) reported a temperature-independent linear velocity–density relationship up to 1020 K. On the other hand, the IXS data of Liu et al. (2014) were systematically higher than our results both at 300 K and at higher temperatures. The density derivative of the IXS data of Liu et al. (2014) was also greater than that of our results, whereas the effects of temperature were almost consistent, e.g., 2.2% and 2.4%

decreases in the present study and the IXS data of Liu et al. (2014), respectively, from 300 K to 700 K at 8000 kg/m^3. The exact reason for the difference between the results of the present study and the IXS data (even between IXS studies (Liu et al. 2014; Antonangeli et al. 2015)) is unclear. Liu et al. (2014) stated that their Fe sample did not contain any detectable chemical impurities according to electron microprobe analyses, although the actual chemical composition was not shown. Antonangeli et al. (2015) reported that the upper limit for possible carbon inclusion in their samples was about 0.6 wt% carbon. It was shown that the presence of carbon increased the value of V_P and decreased the density of Fe (Fiquet et al. 2009), similar to the effects of oxygen (Badro et al. 2007). However, Antonangeli et al. (2015) concluded that the incorporation of carbon had negligible effects on the measured velocities and densities because their velocities and densities for *fcc*-Fe were consistent with results obtained in another study at ambient pressure and high temperature (Zarestky and Stassis 1987). The sample of Decremps et al. (2014) was deposited iron, the chemical composition of which was not shown. Because the chemical compositions of those Fe samples seem not to show clear difference to influence the sound velocity and density, the chemical composition might not explain the disagreement between the results of the present study and previous IXS studies.

Another possible explanation for these differences is the possible frequency dependence of sound velocity. Ultrasonic measurements, including this study, are usually performed at MHz frequencies, whereas the frequencies used for picosecond acoustics are GHz (e.g., Decremps et al. 2014), and for IXS, exceed THz (e.g., Fiquet et al. 2004; Liu et al. 2014). The agreement on absolute values of V_P between the present study and picosecond acoustics (Decremps et al. 2014) and disagreement between the present study and the IXS study (Liu et al. 2014) might indicate that the frequency dependence of V_P becomes marked over THz. Furthermore, the differences in the density evolution for V_P in the present study and that of Liu et al. (2014) might suggest that the frequency dependence also exhibits a density (or pressure) dependence. However, many factors (grain size, impurities, etc.) could affect the frequency dependence. To clarify the frequency dependence and its density (or pressure) dependence, further careful measurements (e.g., using the same grain size and pure samples with various frequencies) are required.

Comparison with the temperature dependence for ε-FeSi

Very limited numbers of high-pressure and high-temperature data sets are available for both V_P and V_S for Fe alloys and Fe compounds. Whitaker et al. (2009) carried out ultrasonic measurements for polycrystalline ε-FeSi (cubic B20 structure) up to 8 GPa and 1273 K. The reported values of V_P and V_S for ε-FeSi as a function of density are plotted in Fig. 10. For ε-FeSi, the values of V_S decreased as the temperature increased at a constant density, which agreed with our results for *bcc*-Fe, but the temperature depression was smaller than that obtained in our study, e.g., only 1.9% from 308 K to 873 K at 6200 kg/m^3 for ε-FeSi, whereas we determined a depression of 6.0% from 300 K to 800 K at 8000 kg/m^3 for *bcc*-Fe. In contrast, the value of V_P for ε-FeSi was almost constant or increased slightly (at the very least, it did not decrease) as the temperature increased at a constant density, which differed greatly from that for *bcc*-Fe.

Martorell et al. (2013) reported that the sound velocities of Fe would drastically drop near melting temperature (T_m) due to a premelting effect (when $T/T_m > 0.96$). The temperature conditions in this study were $T/T_m < 0.42$ (T_m of Fe reported by Liu and Bassett (1975)), and those of ε-FeSi by Whitaker et al. (2009) were $T/T_m < 0.58$ (T_m of FeSi by Lord et al. (2010)) or $T/T_m < 0.75$ (T_m by Santamaría-Pérez and Boehler (2008)). As such, the premelting effect would not be significant for both measurements of *bcc*-Fe and ε-FeSi.

We considered the difference in the effect of temperature on the sound velocity–density relationship for V_P ($=\sqrt{(K_S + 4G/3)/\rho}$) between *bcc*-Fe and ε-FeSi to be attributable, possibly, to the different effects of temperature on the K_S–density relationship. Figures 11b and 11d show that for both *bcc*-Fe and ε-FeSi, respectively, *G* decreased as the temperature increased at a constant density, but the high-temperature K_S behavior at a constant density was extremely different between *bcc*-Fe and ε-FeSi (Figs. 11a and 11c, respectively). The value of K_S for *bcc*-Fe appeared to change in a linear manner with density, regardless of the temperature (Fig. 11a), whereas that for ε-FeSi increased with temperature at a constant density (Fig. 11c).

The difference in the behavior of K_S between *bcc*-Fe and ε-FeSi at a constant density may have been due to differences in the value of $(\partial P/\partial T)_V$ related to thermal pressure ΔP_{th}. For example, for *bcc*-Fe at 8000 kg/m^3, we found that the pressure increased from 2 GPa to 3 GPa (ΔP_{th} = 1 GPa) as the temperature increased from 300 K to 800 K (ΔT = 500 K). However, for ε-FeSi at 6200 kg/m^3, the pressure increased from 1 GPa to 5 GPa (ΔP_{th} = 4 GPa) as the temperature increased from 308 K to 873 K (ΔT = 565 K) according to a previous study (Whitaker et al. 2009), which is much larger than the thermal pressure for *bcc*-Fe. Thus, for ε-FeSi, the increase in K_S induced by the effect of pressure was considered to be larger than the decrease due to the effect of temperature (i.e., $\partial K_S/\partial P \times \Delta P_{th} + \partial K_S/\partial T \times \Delta T > 0$), and K_S increased with temperature at a constant density (Fig. 11c).

In contrast, the value of K_S for *bcc*-Fe was almost constant because the effects of pressure and temperature on K_S were thought to cancel each other out at a constant density (i.e., $\partial K_S/\partial P \times \Delta P_{th} + \partial K_S/\partial T \times \Delta T \approx 0$) (Fig. 11a).

Therefore, under the pressure and temperature conditions analyzed in this study, the velocity–density relationship of V_P for ε-FeSi had an almost negligible dependence on temperature because the effects of temperature on K_S and G at a constant density balanced each other out, and that for *bcc*-Fe was negative in the same manner as the behavior of G.

Implications

We may qualitatively predict the effects of temperature on the sound velocity (V_P)–density relationship based on the degree of thermal pressure for Fe and Fe compounds. The fundamental thermodynamic relationship gives $(\partial P/\partial T)_V = \alpha K_T$. αK_T is correlated with the thermal pressure ΔP_{th} according to the following relationship (Anderson et al. 1989).

$$\Delta P_{\mathrm{th}} = P_{\mathrm{th}}(V,T) - P_{\mathrm{th}}(V,300)$$

$$= \left[\alpha K_{\mathrm{T}}(V_{300},T) + \left(\frac{\partial K_{\mathrm{T}}}{\partial T}\right)_V \ln\left(\frac{V_{300}}{V}\right)\right](T-300) \quad (8)$$

Zhang and Guyot (1999) reported $\alpha K_T(V_{300},T) = 6.5(1) \times 10^{-3}$ GPa/K for *bcc*-Fe. For ε-FeSi, we fitted the data reported by Guyot et al. (1997) using equation (8) to estimate $\alpha K_T(V_{300},T)$ as $7.6(1) \times 10^{-3}$ GPa/K. We simply assumed that when $\alpha K_T(V_{300},T)$ for Fe compounds < ~7 × 10^{-3} GPa/K (intermediate between $6.5(1) \times 10^{-3}$ and $7.6(1) \times 10^{-3}$), then the effect of temperature on the V_P–density relationship is negative, similar to *bcc*-Fe. In contrast, the effect is small or negligible when $\alpha K_T(V_{300},T) > \sim 7 \times 10^{-3}$ GPa/K, similar to ε-FeSi.

Yamazaki et al. (2012) reported a valuable pressure–volume–temperature data set for *hcp*-Fe up to 80 GPa and 1900 K. After fitting these data using equation (8), we obtained $\alpha K_T(V_{300},T) = 12(1) \times 10^{-3}$ GPa/K. This indicates that the effect of temperature on the V_P–density relationship might be quite small for *hcp*-Fe, as found for ε-FeSi. This small effect of temperature was also reported for *hcp*-Fe in previous IXS studies by Antonangeli et al. (2012) and Ohtani et al. (2013). To discuss the temperature effect on the V_P–density relationship for *hcp*-Fe quantitatively based on experimental results, higher temperature conditions (> 2000 K) may be necessary.

For iron–sulfur compounds, Fe_3S, we estimated $\alpha K_T(V_{300},T)$ to be $15(2) \times 10^{-3}$ GPa/K after fitting the thermal pressure data given by Seagle et al. (2006) using equation (8), thereby implying a small effect of temperature on the V_P–density relationship. Gao et al.

(2011) reported V_P and V_S data for Fe_3C up to 47 GPa and 1450 K using NRIXS. It is difficult to verify the quantitative effect of temperature on the velocity–density relationship for Fe_3C due to the limited data available, but V_S appears to decrease as the temperature increases at a constant density, whereas the effect of temperature on V_P falls within the uncertainty of measurements. Using the pressure–volume–temperature data for Fe_3C given by Litasov et al. (2013), we estimated $\alpha K_T(V_{300},T)$ to be $2.6(3) \times 10^{-3}$ GPa/K and $8.9(1) \times 10^{-3}$ GPa/K for ferromagnetic and paramagnetic Fe_3C, respectively. Thus, ferromagnetic Fe_3C might exhibit a clear negative effect of temperature on the V_P–density relationship, whereas paramagnetic Fe_3C might exhibit a small effect.

hcp-Fe, Fe_3S, and paramagnetic Fe_3C with large αK_T values are high-pressure phases, and ferromagnetic Fe_3C and *bcc*-Fe with small αK_T values are low-pressure phases. These results imply that a high-pressure phase may generally exhibit a small temperature effect on the V_P–density relationship. Therefore, at ultra-high pressures pertinent to Earth's core conditions, the effects of temperature on the V_P–density relationship for Fe alloys might be small regardless of light element contents. However, it should be noted that the aforementioned discussion of the effects of temperature on the V_P–density relationship for Fe compounds is still speculative. Thus, to achieve a more quantitative analysis of the effects of temperature, further sound velocity measurements (of both V_P and V_S) are required under a wide range of pressure and temperature conditions with various compositions. Understanding differences and/or common points regarding the effects of temperature on the sound velocity–density relationship for various Fe alloys and compounds will be important for constraining the abundances of light elements in planetary cores and for elucidating planetary interiors.

Acknowledgements

We thank Y. Nakajima for useful suggestions and discussions. We also thank Y. Ito for chemical analysis. This work was supported by JSPS KAKENHI Grant Numbers 26887006 and 15K17784 for YS and 22000002 for EO. This work was carried out under the Visiting Researcher's Program of Geodynamics Research Center, Ehime University (PRIUS). The synchrotron radiation experiments were performed at the BL04B1 beamline at the SPring-8 facility with the approval of the Japan Synchrotron Radiation Research Institute (JASRI) (proposal nos. 2014A1472 and 2014B1378).

References cited

Adams, J.J., Agosta, D.S., Leisure, R.G., and Ledbetter, H. (2006) Elastic constants of monocrystal iron from 3 to 500 K. Journal of Applied Physics, 100, 113530.

Anderson, O.L., Isaak, D.G., and Yamamoto, S. (1989) Anharmonicity and the equation of state for gold. Journal of Applied Physics, 65, 1534–1543.

Antonangeli, D., Komabayashi, T., Occelli, F., Borissenko, E., Walters, A.C., Fiquet, G., and Fei, Y. (2012) Simultaneous sound velocity and density measurements of hcp iron up to 93 GPa and 1100 K: An experimental test of the Birch's law at high temperature. Earth and Planetary Science Letters, 331–332, 210–214.

Antonangeli, D., Morard, G., Schmer, N.C., Komabayashi, T., Krisch, M., Fiquet, G., and Fei, Y. (2015) Toward a mineral physics reference model for the Moon's core. Proceedings of the National Academy of Sciences, 112, 3916–3919.

Antonangeli, D., Siebert, J., Badro, J., Farber, D.L., Fiquet, G., Morard, G., and Ryerson, F.J. (2010) Composition of the Earth's inner core from high-pressure sound velocity measurements in Fe-Ni-Si alloys. Earth and Planetary Science Letters, 295, 292–296.

Antonangeli, D., and Ohtani, E. (2015) Sound velocity of hcp-Fe at high pressure: experimental constraints, extrapolations and comparison with seismic models. Progress in Earth and Planetary Science, 2, 3, doi:10.1186/s40645-015-0034-9.

Badro, J., Fiquet, G., Guyot, F., Gregoryanz, E., Occelli, F., Antonangeli, D., and d'Astuto, M. (2007) Effect of light elements on the sound velocities in solid iron: implications for the composition of Earth's core. Earth and Planetary Science Letters, 254, 233–238.

Birch, F. (1952) Elasticity and constitution of the Earth's interior. Journal of Geophysical Research, 52, 227–286.

Birch, F. (1961) Composition of the Earth's mantle. Geophysical Journal of the Royal Astronomical Society, 4, 295–311.

Brown, J.M., and McQueen, R.G. (1986) Phase transitions, Grüneisen parameter, and elasticity for shocked iron between 77 GPa and 400 GPa. Journal of Geophysical Research, 91, 7485–7494.

Bundy, F.P. (1965) Pressure-temperature phase diagram of iron to 200 kbar, 900 °C. Journal of Applied Physics, 36, 616–620.

Claussen, W.F. (1960) Detection of the α-γ iron phase transformation by differential thermal conductivity analysis. Review of Scientific Instruments, 31, 878–881.

Decremps, F., Antonangeli, D., Gauthier, M., Ayrinhac, S., Morard, M., Le Marchand, G., Bergame, F., and Philippe, J. (2014) Sound velocity of iron up to 152 GPa by picosecond acoustics in diamond anvil cell. Geophysical Research Letters, 41, 1459–1464.

Dever, D.J. (1972) Temperature dependence of the elastic constants in αiron single crystals: relationship to spin order and diffusion anomalies. Journal of Applied Physics, 43, 3293–3301.

Dumberry, M., and Rivoldini, A. (2015) Mercury's inner core size and core-crystallization regime. Icarus, 248, 254–268.

Dziewonski, A.M., and Anderson, D.L. (1981) Preliminary reference Earth model. Physics of the Earth and Planetary Interiors, 25, 297–356.

Fei, Y., Ricolleau, A., Frank, M., Mibe, K., Shen, G., and Prakapenka, V. (2007) Toward an internally consistent pressure scale. Proceedings of the National Academy of Sciences, 104, 9182–9186.

Fiquet, G., Badro, J., Gregoryanz, E., Fei, Y., and Occelli, F. (2009) Sound velocity in iron carbide (Fe_3C) at high pressure: implications for the carbon content of the Earth's inner core. Physics of the Earth and Planetary Interiors, 172, 125–129.

Fiquet, G., Badro, J., Guyot, F., Bellin, Ch., Krisch, M., Antonangeli, D., Requardt, H., Mermet, A., Farber, D., Aracne-Ruddle, A., and Zhang, J. (2004) Application of inelastic X-ray scattering to the measurements of acoustic wave velocities in geophysical materials at very high pressure. Physics of the Earth and Planetary Interiors, 143–144, 5–18.

Fiquet, G., Badro, J., Guyot, F., Requardt, H., and Krisch, M. (2001) Sound velocities in iron to 110 gigapascals. Science, 291, 468–471.

Gao, L., Chen, B., Wang, J., Alp, E.E., Zhao, J., Lerche, M., Sturhahn, W., Scott, H.P., Huang, F., Ding, Y., Sinogeikin, S.V., Lundstrom, C.C., Bass, J.D., and Li, J. (2008) Pressure-induced magnetic transition and sound velocities of Fe_3C: Implications for carbon in the Earth's inner core. Geophysical Research Letters, 35, L17306, doi:10.1029/2008GL034817.

Gao, L., Chen, B., Zhao, J., Alp, E.E., Sturhahn, W., and Li, J. (2011) Effect of temperature on sound velocities of compressed Fe_3C, a candidate component of the Earth's inner core. Earth and Planetary Science Letters, 309, 213–220.

Guinan, M.W., and Beshers, D.N. (1968) Pressure derivatives of the elastic constants of α-iron to 10 kbs. Journal of Physics and Chemistry of Solids, 29, 541–549.

Guyot, F., Zhang, J., Martinez, I., Matas, J., Ricard, Y., and Javoy, M. (1997) P-V-T measurements of iron silicide (ε-FeSi): Implications for silicate-metal interactions in the early Earth. European Journal of Mineralogy, 9, 277–285.

Higo, Y., Kono, Y., Inoue, T., Irifune, T., and Funakoshi, K. (2009) A system for measuring elastic wave velocity under high pressure and high temperature using a combination of ultrasonic measurement and the multi-anvil apparatus at SPring-8. Journal of Synchrotron Radiation, 16, 762–768.

Huang, E., Bassett, W.A., and Tao, P. (1987) Pressure-temperature-volume relationship for hexagonal close packed iron determined by synchrotron radiation. Journal of Geophysical Research, 92, 8129–8135.

Ichikawa, H., Tsuchiya, T., and Tange, Y. (2015) The P-V-T equation of state and thermodynamic properties of liquid iron. Journal of Geophysical Research, 119, 240–252.

Isaak, D.G., and Masuda, K. (1995) Elastic and viscoelastic properties of α iron at high temperatures. Journal of Geophysical Research, 100, 17689–17698.

Kamada, S., Ohtani, E., Fukui, H., Sakai, T., Terasaki, H., Takahashi, S., Shibazaki, Y., Tstsui, S., Baron, A.Q.R., Hirao, N., and Ohishi, Y. (2014) The sound velocity measurements of Fe_3S. American Mineralogist, 99, 98–101.

Kantor, A.P., Kantor, I.Y., Kurnosov, A.V., Kuznetsov, A.Y., Dubrovinskaia, N.A., Krisch, M., Bossak, A.A., Dmitriev, V.P., Urusov, V.S., and Dubrovinsky, L.S. (2007) Sound wave velocities of fcc Fe-Ni alloy at high pressure and temperature by mean of inelastic X-ray scattering. Physics of the Earth and Planetary Interiors, 164, 83–89.

Klotz, S., and Braden, M. (2000) Phonon dispersion of bcc iron to 10 GPa. Physical Review Letters, 85, 3209–3212.

Leese, J., and Lord, Jr., A.E. (1968) Elastic stiffness coefficients of single-crystal iron from room temperature to 500 °C. Journal of Applied Physics, 30, 3986–3988.

Li, Y., and Fei, Y. (2014) Experimental constraints on core composition. In R.W. Carlson, Eds., The mantle and core, Treatise on geochemistry, 2nd ed., vol. 3, p. 527–557. Elsevior, U.K.

Lin, J.-F., Fei, Y., Sturhahn, W., Zhao, J., Mao, H.-K., and Hemley, R.J. (2004) Magnetic transition and sound velocities of Fe_3S at high pressure: Implications for Earth and planetary cores. Earth and Planetary Science Letters, 226, 33–40.

Lin, J.-F., Struzhkin, V.V., Sturhahn, W., Huang, E., Zhao, J., Hu, M.Y., Alp, E.E., Mao, H.-K., Boctor, N., and Hemley, R.J. (2003) Sound velocities of iron-nickel and iron-silicon alloys at high pressures. Geophysical Research Letters, 30, 2112, doi:10.1029/2003GL018405.

Lin, J.-F., Sturhahn, W., Zhao, J., Shen, G., Mao, H.-K., and Hemley, R.J. (2005) Sound velocities of hot dense iron: Birch's law revisited. Science, 308, 1892–1894.

Litasov, K.D., Sharygin, I.S., Dorogokupets, P.I., Shatskiy, A., Gavryushkin, P.N., Sokolova, T.S., Ohtani, E., Lie, J., and Funakoshi, K. (2013) Thermal equation of state and thermodynamic properties of iron carbide Fe_3C to 31 GPa and 1473 K. Journal of Geophysical Research, 118, 1–11.

Liu, J., Lin, J.-F., Alatas, A., and Bi, W. (2014) Sound velocities of bcc-Fe and $Fe_{0.85}Si_{0.15}$ alloy at high pressure and temperature. Physics of the Earth and Planetary Interiors, 233, 24–32.

Liu, L.-G., and Bassett, W.A. (1975) The melting of iron up to 200 kbar. Journal of Geophysical Research, 80, 3777–3782.

Lord, O.T., Walter, M.J., Dobson, D.P., Armstrong, L., Clark, S.M., and Kleppe, A. (2010) The FeSi phase diagram to 150 GPa. Journal of Geophysical Research, 115, B06208, doi:10.1029/2009JB006528.

Mao, H.-K., Bassett, W.A., and Takahashi, T. (1967) Effect of pressure on crystal structure and lattice parameters of iron up to 300 kbar. Journal of Applied Physics, 38, 272–276.

Mao, H.-K., Xu, J., Struzhkin, V.V., Shu, J., Hemley, R.J., Sturhahn, W., Hu, M.Y., Alp, E.E., Vočadlo, L., Alfè, D., Price, G.D., Gillan, M.J., Schwoerer-Böhning, M., Häusermann, D., Eng, P., Shen, G., Giefers, H., Lübbers, R., and Wortmann, G. (2001) Phonon density of states of iron up to 153 gigapascals. Science, 292, 914–916.

Mao, Z., Lin, J.-F., Liu, J., Alatas, A., Gao, L., Zhao, J., and Mao, H.-K. (2012) Sound velocities of Fe and Fe-Si alloy in the Earth's core. Proceedings of the National Academy of Sciences, 109, 10239–10244.

Martorell, B., Vočadlo, L., Brodholt, J., and Wood, I.G. (2013) Strong premelting effect in the elastic properties of hcp-Fe under inner-core conditions. Science, 342, 466–468.

Murphy, C.A., Jackson, J.M., and Sturhahn, W. (2013) Experimental constraints on the thermodynamics and sound velocities of hcp-Fe to core pressures. Journal of Geophysical Research, 118, 1999–2016.

Ohtani, E., Shibazaki, Y., Sakai, T., Mibe, K., Fukui, H., Kamada, S., Sakamaki, T., Seto, T., Tsutsui, S., and Baron, A.Q.R. (2013) Sound velocity of hexagonal close-packed iron up to core pressures. Geophysical Research Letters, 40, 1–6.

Poirier, J.-P. (1994) Light elements in the Earth's outer core: A critical review. Physics of the Earth and Planetary Interiors, 85, 319–337.

Quareni, F., and Mulargia, F. (1988) The validity of the common approximate expressions for the Grüneisen parameter. Geophysical Journal, 93, 505–519.

Rotter, C.A., and Smith, C.S. (1966) Ultrasonic equation of state of iron: I. low pressure, room temperature. Journal of Physics and Chemistry of Solids, 27, 267–276.

Santamaría-Pérez, D., and Boehler, R. (2008) FeSi melting curve up to 70 GPa. Earth and Planetary Science Letters, 265, 743–747.

Seagle, C.T., Campbell, A.J., Heinz, D.L., Shen, G., and Prakapenka, V.B. (2006) Thermal equation of state of Fe_3S and implications for sulfur in Earth's core. Journal of Geophysical Research, 111, B06209, doi:10.1029/2005JB004091.

Sha, X., and Cohen, R.E. (2010) Elastic isotropy of ε-Fe under Earth's core conditions. Geophysical Research Letters, 37, L10302, doi:10.1029/2009GL042224.

Shibazaki, Y., Ohtani, E., Fukui, H., Sakai, T., Kamada, S., Ishikawa, D., Tsutsui, S., Baron, A.Q.R., Nishitani, N., Hirao, N., and Takemura, K. (2012) Sound velocity measurements in dhcp-FeH up to 70 GPa with inelastic X-ray scattering: Implications for the composition of the Earth's core. Earth and Planetary Science Letters, 313–314, 79–85.

Takahashi, T., Bassett, W.A., and Mao, H.-K. (1968) Isothermal compression of the alloys of iron up to 300 kilobars at room temperature: Iron-nickel alloys. Journal of Geophysical Research, 73, 4717–4725.

Tange, Y., Nishihara, Y., and Tsuchiya, T. (2009) Unified analyses for P-V-T equation of state of MgO: A solution for pressure-scale problems in high P-T experiments. Journal of Geophysical Research, 114, B03208, doi:10.1029/2008JB005813.

Vočadlo, L., Dobson, D.P., and Wood, I.G. (2009) Ab initio calculations of the elasticity of hcp-Fe as a function of temperature at inner-core pressure. Earth and Planetary Science Letters, 288, 534–538.

Wakabayashi, D., and Funamori, N. (2015) Solving the problem of inconsistency in reported equations of state for h-BN. High Pressure Research, 35, 123–129.

Whitaker, M.L., Liu, W., Liu, Q., Wang, L., and Li, B. (2009) Thermoelasticity of ε-FeSi to 8 GPa and 1273 K. American Mineralogist, 94, 1039–1044.

Wilburn, D.R., and Bassett, W.A. (1978) Hydrostatic compression of iron and related compounds: an overview. American Mineralogist, 63, 591–596.

Yamazaki, D., Ito, E., Yoshino, T., Yoneda, A., Guo, X., Zhang, B., Sun, W., Shimojuku, A., Tsujino, N., Kunimoto, T., Higo, Y., and Funakoshi, K. (2012) P-V-T equation of state for ε-iron up to 80 GPa and 1900 K using the Kawai-type high pressure apparatus equipped with sintered diamond anvils. Geophysical Research Letters, 39, L20308, doi:10.1029/2012GL053540.

Zaresky, J., and Stassis, C. (1987) Lattice dynamics of γ-Fe. Physical Review B*, 35,* 4500–4502.

Zhang, J., and Guyot, F. (1999) Thermal equation of state of iron and $Fe_{0.91}Si_{0.09}$. Physics and Chemistry of Minerals, 26, 206–211.

Zharkov, V.N., Gudkova, T.V., and Molodensky, S.M. (2009) On models of Mars' interior and amplitudes of forced nutations: 1. the effects of deviation of Mars from its equilibrium state on the flattening of the core-mantle boundary. Physics of the Earth and Planetary Interiors, 172, 324–334.

Figure captions

Fig. 1. Schematic illustrations of cell assemblies used for: (a) simultaneous sound velocity

and density measurements and (b) thermocouple (TC) tests.

Fig. 2. Diffraction patterns obtained from the samples at ambient conditions (0 GPa and 300 K) and at the highest pressure (6.3 GPa and 640 K).

Fig. 3. Examples of: (a) P- and (b) S-wave signals observed at 6.3 GPa and 640 K.

Fig. 4. Pressure–volume–temperature data obtained in this study (solid circles), together with the equation of state for *bcc*-Fe reported by Zhang and Guyot (1999) (gray lines) and previous IXS studies (open squares, Liu et al. (2014); open stars, Antonangeli et al. (2015)).

Fig. 5. (a) V_P and (b) V_S, obtained as a function of pressure, for polycrystalline *bcc*-Fe in this study (solid circles), together with previous IXS data (open squares, Liu et al. (2014); open stars, Antonangeli et al. (2015)), picosecond acoustics (PA) at frequencies of about 100 GHz (Decremps et al. 2014) (open down triangles), and ambient-pressure results for *bcc*-Fe single-crystal, measured using an ultrasonic technique at frequencies of 20–70 MHz (Dever 1972) (open diamonds). The pressure values for the IXS studies were re-estimated

based on the equation of state for *bcc*-Fe reported by Zhang and Guyot (1999). Those for picosecond acoustics were measured using ruby fluorescence (Decremps et al. 2014). The error bars fall within symbols for the data of Decremps et al. (2014).

Fig. 6. Calculated adiabatic (a) bulk (K_S) and (b) shear (G) moduli obtained in this study, as a function of pressure, with the fitting lines at each temperature (300 K, 400 K, 500 K, 600 K, and 700 K) for polycrystalline *bcc*-Fe.

Fig. 7. (a) Temperature dependences obtained in this study for V_P, V_S, and V_Φ at approximately 2–3 GPa for polycrystalline *bcc*-Fe. (b) Temperature dependences obtained in this study for K_S, G, and ρ at approximately 2–3 GPa, together with K_S and G from a previous ambient-pressure study (Dever 1972). The vertical axis shows the value normalized against that at 300 K. Lines are provided as guides.

Fig. 8. V_P and V_S as functions of density with the fitted lines. The solid circles and open diamonds denote the results obtained in the present study (polycrystalline *bcc*-Fe) and previously reported ambient pressure results (*bcc*-Fe single-crystal) (Dever 1972),

respectively. The extrapolation of the lines obtained in the present study for V_S to ambient pressure agreed well with the ambient data (Dever 1972). The lines for V_P were slightly lower than the ambient data, but they were consistent within errors for velocity and temperature.

Fig. 9. Comparison of the dependences of V_P on density and temperature for polycrystalline *bcc*-Fe according to the present ultrasonic study and previous picosecond acoustics (PA) (Decremps et al. 2014) and IXS studies (Liu et al. 2014; Antonangeli et al. 2015). Densities of Decremps et al. (2014) were estimated based on the equation of state of *bcc*-Fe reported by Zhang and Guyot (1999). The solid lines are the fitted lines obtained in the present study at 300 K, 500 K, and 700 K. The dotted lines represent the IXS results obtained by Liu et al. (2014). The open down triangles and stars denote the PA (Decremps et al. 2014) and IXS (Antonangeli et al. 2015) results, respectively. The typical errors of this study and Liu et al. (2014) are shown in the insert figure. The error bars fall within symbols for the data of Decremps et al. (2014).

Fig. 10. V_P and V_S as functions of density for polycrystalline ε-FeSi, obtained by Whitaker

et al. (2009).

Fig. 11. (a) K_S and (b) G as functions of density for polycrystalline *bcc*-Fe in the present study, and previously reported results for (c) K_S and (d) G for polycrystalline *ε*-FeSi (Whitaker et al. 2009).

Table 1. Experimental pressures (*P*) and temperatures (*T*), and determined unit-cell volume (*V*), density (*ρ*), P- (V_P) and S-wave (V_S), and bulk sound ($V_Φ$) velocities, and adiabatic bulk (K_S), shear (*G*), and isothermal bulk (K_T) moduli for *bcc*-Fe.

P (GPa)[a]	*T* (K)[a]	*V* ($Å^3$)	*ρ* (kg/m^3)	V_P (m/s)	V_S (m/s)	$V_Φ$ (m/s)	K_S (GPa)	*G* (GPa)	K_T (GPa)
3.0(5)	814(84)	23.57(2)	7872(5)	5705(59)	-	-	-	-	-
2.7(5)	706(78)	23.54(3)	7881(9)	5786(58)	3066(31)	4576(77)	165.1(57)	74.1(15)	156.8(55)
2.4(5)	544(72)	23.43(1)	7917(4)	5881(62)	3147(33)	4624(84)	169.3(62)	78.4(17)	162.7(60)
2.2(5)	409(67)	23.28(4)	7968(13)	5955(60)	3210(33)	4660(83)	173.0(61)	82.1(17)	167.9(60)
2.0(5)	300[b]	23.26(2)	7976(5)	6018(61)	3262(33)	4693(84)	175.7(63)	84.9(17)	171.8(61)
4.5(5)	651(84)	23.11(2)	8028(8)	5969(50)	3120(26)	4759(67)	181.8(51)	78.1(13)	173.4(50)
4.5(5)	620(82)	23.07(1)	8042(4)	5998(51)	3147(27)	4772(68)	183.1(52)	79.6(14)	175.1(51)
4.2(5)	536(78)	23.06(2)	8045(7)	6030(52)	3185(27)	4779(69)	183.7(53)	81.6(14)	176.7(52)
4.0(5)	421(73)	22.97(1)	8076(2)	6090(51)	3244(27)	4801(69)	186.1(54)	85.0(14)	180.5(53)
3.7(5)	309(68)	22.89(2)	8105(6)	6146(59)	3274(31)	4846(79)	190.4(62)	86.9(17)	186.1(62)
6.3(5)	635(91)	22.79(2)	8142(6)	6087(51)	3193(27)	4843(68)	191.0(54)	83.0(14)	182.4(53)
5.8(5)	503(82)	22.74(3)	8158(10)	6113(65)	3207(34)	4863(87)	192.9(69)	83.9(18)	186.0(67)
5.5(5)	367(75)	22.71(1)	8169(4)	6193(61)	3275(32)	4905(82)	196.5(66)	87.6(17)	191.3(65)
5.4(2)	300[b]	22.68(2)	8180(8)	6255(52)	3332(28)	4933(70)	199.0(57)	90.8(15)	194.7(56)

Number in parenthesis represents the uncertainties in the last digit.

[a] Most of uncertainties in pressures and temperatures originate in uncertainties in equation of state for hBN (Wakabayashi and Funamori 2015).

[b] Fixed values.

Table 2. Comparison of elastic parameters for *bcc*-Fe.

P range	*T* range	K_{S0}	$\partial K_{S0}/\partial P$	$\partial K_{S0}/\partial T$	G_0	$\partial G_0/\partial P$	$\partial G_0/\partial T$	K_{T0}	$\partial K_{T0}/\partial P$	$\partial K_{T0}/\partial T$	Method	Sample	Ref.[a]
(GPa)	(K)	(GPa)		(GPa/K)	(GPa)		(GPa/K)	(GPa)		(GPa/K)			
2.0–6.3	300–800	163.2(15)	6.75(33)	-0.038(3)	81.4(6)	1.66(14)	-0.029(1)	159.9(15)	6.52(32)	-0.049(3)	Ultrasonic	Polycrystal	This study
2.0–6.3	300–800	166.1(9)	6[b]	-0.037(4)	80.4(3)	1.9[b]	-0.029(1)	163.8(10)	5.5[b]	-0.048(4)	Ultrasonic	Polycrystal	This study
0–0.36	300	166.9	5.97	-	81.8[c]	1.91	-	-	-	-	Ultrasonic	Single	1
0–1	300	166.4	5.29	-	81.4[c]	1.82	-	-	-	-	Ultrasonic	Single	2
0	298–773	168.7	-	-0.041	72.1[c]	-	-0.015	-	-	-	Ultrasonic	Single	3
0	298–773	167.8	-	-0.035	82.0[c]	-	-0.029	-	-	-	Ultrasonic	Single	4
0	298–800	165.7	-	-0.046	82.0[c]	-	-0.034	-	-	-	Ultrasonic	Single	5
0	300–500	166.2	-	-0.029	81.5[c]	-	-0.025	-	-	-	Ultrasonic	Single	6
0-10	300	159.0	-	-	77.9[c]	-	-	-	-	-	INS[d]	Single	7
0–15	296	-	-	-	-	-	-	156.3	5.62	-	XRD[d]	Polycrystal	8
0–30	296	-	-	-	-	-	-	162	5.5	-	XRD	Polycrystal	9
0–11	298	-	-	-	-	-	-	164	4[b]	-	XRD	Polycrystal	10
0–12	298–723	-	-	-	-	-	-	171	4[b]	-0.010	XRD	Polycrystal	11
0–9	298–774	-	-	-	-	-	-	159	4[b]	-0.043	XRD	Polycrystal	12

Number in parenthesis represents the uncertainties in the last digit.

[a] References: 1 = Rotter and Smith (1966); 2 = Guinan and Beshers (1968); 3 = Leese and Lord (1968); 4 = Dever (1972); 5 = Isaak and Masuda (1995); 6 = Adams et al. (2006); 7 = Klotz and Braden (2000); 8 = Mao et al. (1967); 9 = Takahashi et al. (1968); 10 = Wilburn and Bassett (1978); 11 = Huang et al. (1987); 12 = Zhang and Guyot (1999).

[b] Fixed values.

[c] Voight-Reuss-Hill average.

[d] INS = inelastic neutron scattering; XRD = X-ray diffraction.

Table 1. Experimental pressures (*P*) and temperatures (*T*), and determined unit-cell volume (*V*), density (*ρ*), P- (V_P) and S-wave (V_S), and bulk sound (V_Φ) velocities, and adiabatic bulk (K_S), shear (*G*), and isothermal bulk (K_T) moduli for *bcc*-Fe.

P (GPa)[a]	*T* (K)[a]	*V* (Å^3)	*ρ* (kg/m^3)	V_P (m/s)	V_S (m/s)	V_Φ (m/s)	K_S (GPa)	*G* (GPa)	K_T (GPa)
3.0(5)	814(84)	23.57(2)	7872(5)	5705(59)	-	-	-	-	-
2.7(5)	706(78)	23.54(3)	7881(9)	5786(58)	3066(31)	4576(77)	165.1(57)	74.1(15)	156.8(55)
2.4(5)	544(72)	23.43(1)	7917(4)	5881(62)	3147(33)	4624(84)	169.3(62)	78.4(17)	162.7(60)
2.2(5)	409(67)	23.28(4)	7968(13)	5955(60)	3210(33)	4660(83)	173.0(61)	82.1(17)	167.9(60)
2.0(5)	300[b]	23.26(2)	7976(5)	6018(61)	3262(33)	4693(84)	175.7(63)	84.9(17)	171.8(61)
4.5(5)	651(84)	23.11(2)	8028(8)	5969(50)	3120(26)	4759(67)	181.8(51)	78.1(13)	173.4(50)
4.5(5)	620(82)	23.07(1)	8042(4)	5998(51)	3147(27)	4772(68)	183.1(52)	79.6(14)	175.1(51)
4.2(5)	536(78)	23.06(2)	8045(7)	6030(52)	3185(27)	4779(69)	183.7(53)	81.6(14)	176.7(52)
4.0(5)	421(73)	22.97(1)	8076(2)	6090(51)	3244(27)	4801(69)	186.1(54)	85.0(14)	180.5(53)
3.7(5)	309(68)	22.89(2)	8105(6)	6146(59)	3274(31)	4846(79)	190.4(62)	86.9(17)	186.1(62)
6.3(5)	635(91)	22.79(2)	8142(6)	6087(51)	3193(27)	4843(68)	191.0(54)	83.0(14)	182.4(53)
5.8(5)	503(82)	22.74(3)	8158(10)	6113(65)	3207(34)	4863(87)	192.9(69)	83.9(18)	186.0(67)
5.5(5)	367(75)	22.71(1)	8169(4)	6193(61)	3275(32)	4905(82)	196.5(66)	87.6(17)	191.3(65)
5.4(2)	300[b]	22.68(2)	8180(8)	6255(52)	3332(28)	4933(70)	199.0(57)	90.8(15)	194.7(56)

Number in parenthesis represents the uncertainties in the last digit.

[a] Most of uncertainties in pressures and temperatures originate in uncertainties in equation of state for hBN (Wakabayashi and Funamori 2015).

[b] Fixed values.

Table 2. Comparison of elastic parameters for *bcc*-Fe.

P range (GPa)	T range (K)	K_{S0} (GPa)	$\partial K_{S0}/\partial P$	$\partial K_{S0}/\partial T$ (GPa/K)	G_0 (GPa)	$\partial G_0/\partial P$	$\partial G_0/\partial T$ (GPa/K)	K_{T0} (GPa)	$\partial K_{T0}/\partial P$	$\partial K_{T0}/\partial T$ (GPa/K)	Method	Sample	Ref.[a]
2.0–6.3	300–800	163.2(15)	6.75(33)	-0.038(3)	81.4(6)	1.66(14)	-0.029(1)	159.9(15)	6.52(32)	-0.049(3)	Ultrasonic	Polycrystal	This study
2.0–6.3	300–800	166.1(9)	6[b]	-0.037(4)	80.4(3)	1.9[b]	-0.029(1)	163.8(10)	5.5[b]	-0.048(4)	Ultrasonic	Polycrystal	This study
0–0.36	300	166.9	5.97	-	81.8[c]	1.91	-	-	-	-	Ultrasonic	Single	1
0–1	300	166.4	5.29	-	81.4[c]	1.82	-	-	-	-	Ultrasonic	Single	2
0	298–773	168.7	-	-0.041	72.1[c]	-	-0.015	-	-	-	Ultrasonic	Single	3
0	298–773	167.8	-	-0.035	82.0[c]	-	-0.029	-	-	-	Ultrasonic	Single	4
0	298–800	165.7	-	-0.046	82.0[c]	-	-0.034	-	-	-	Ultrasonic	Single	5
0	300–500	166.2	-	-0.029	81.5[c]	-	-0.025	-	-	-	Ultrasonic	Single	6
0-10	300	159.0	-	-	77.9[c]	-	-	-	-	-	INS[d]	Single	7
0–15	296	-	-	-	-	-	-	156.3	5.62	-	XRD[d]	Polycrystal	8
0–30	296	-	-	-	-	-	-	162	5.5	-	XRD	Polycrystal	9
0–11	298	-	-	-	-	-	-	164	4[b]	-	XRD	Polycrystal	10
0–12	298–723	-	-	-	-	-	-	171	4[b]	-0.010	XRD	Polycrystal	11
0–9	298–774	-	-	-	-	-	-	159	4[b]	-0.043	XRD	Polycrystal	12

Number in parenthesis represents the uncertainties in the last digit.

[a] References: 1 = Rotter and Smith (1966); 2 = Guinan and Beshers (1968); 3 = Leese and Lord (1968); 4 = Dever (1972); 5 = Isaak and Masuda (1995); 6 = Adams et al. (2006); 7 = Klotz and Braden (2000); 8 = Mao et al. (1967); 9 = Takahashi et al. (1968); 10 = Wilburn and Bassett (1978); 11 = Huang et al. (1987); 12 = Zhang and Guyot (1999).

[b] Fixed values.

[c] Voight-Reuss-Hill average.

[d] INS = inelastic neutron scattering; XRD = X-ray diffraction.

Figure 1

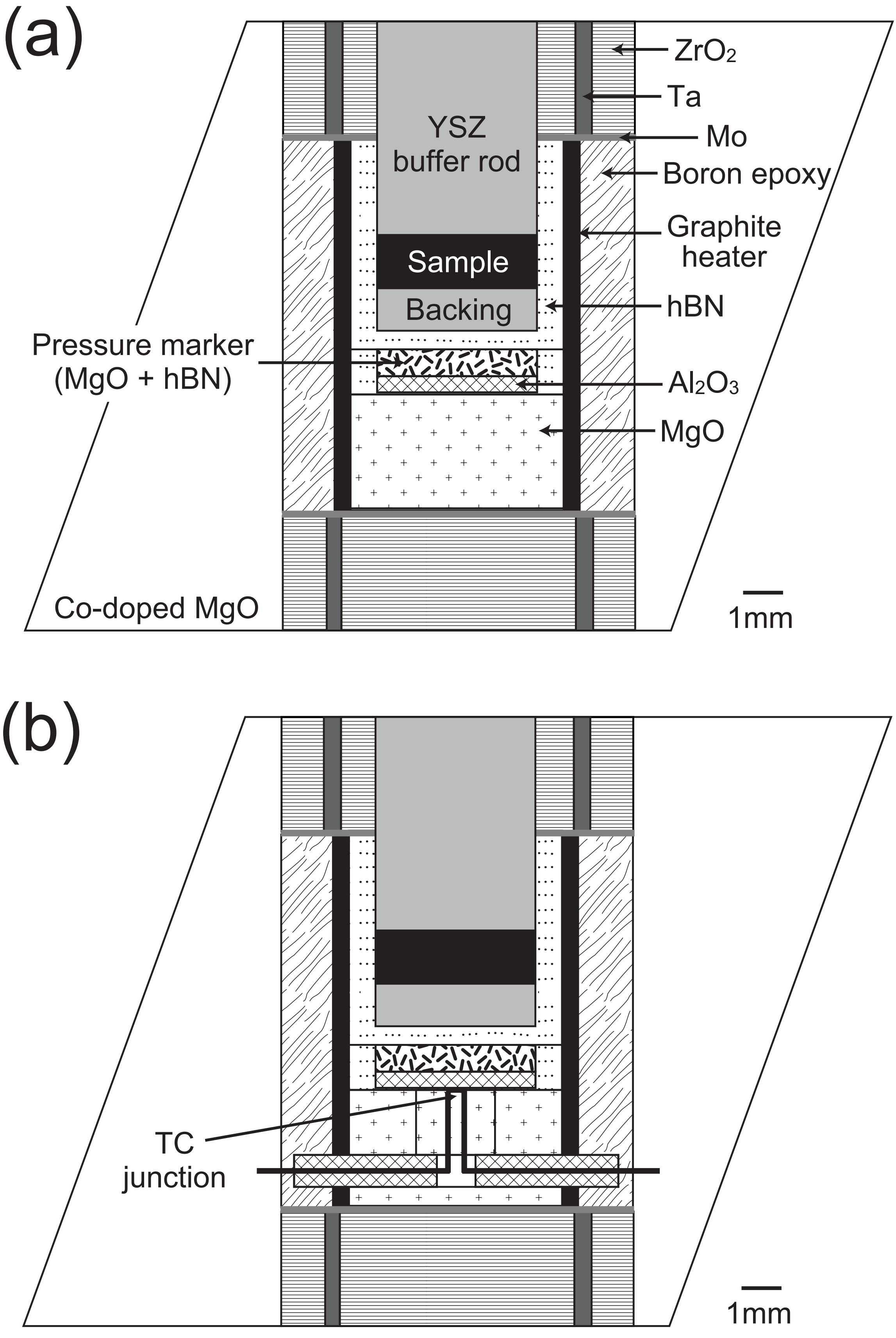

(a)
ZrO2
Ta
Mo
Boron epoxy
Graphite heater
hBN
Al2O3
MgO
YSZ buffer rod
Sample
Backing
Pressure marker (MgO + hBN)
Co-doped MgO
1mm
(b)
TC junction
1mm

Figure 2

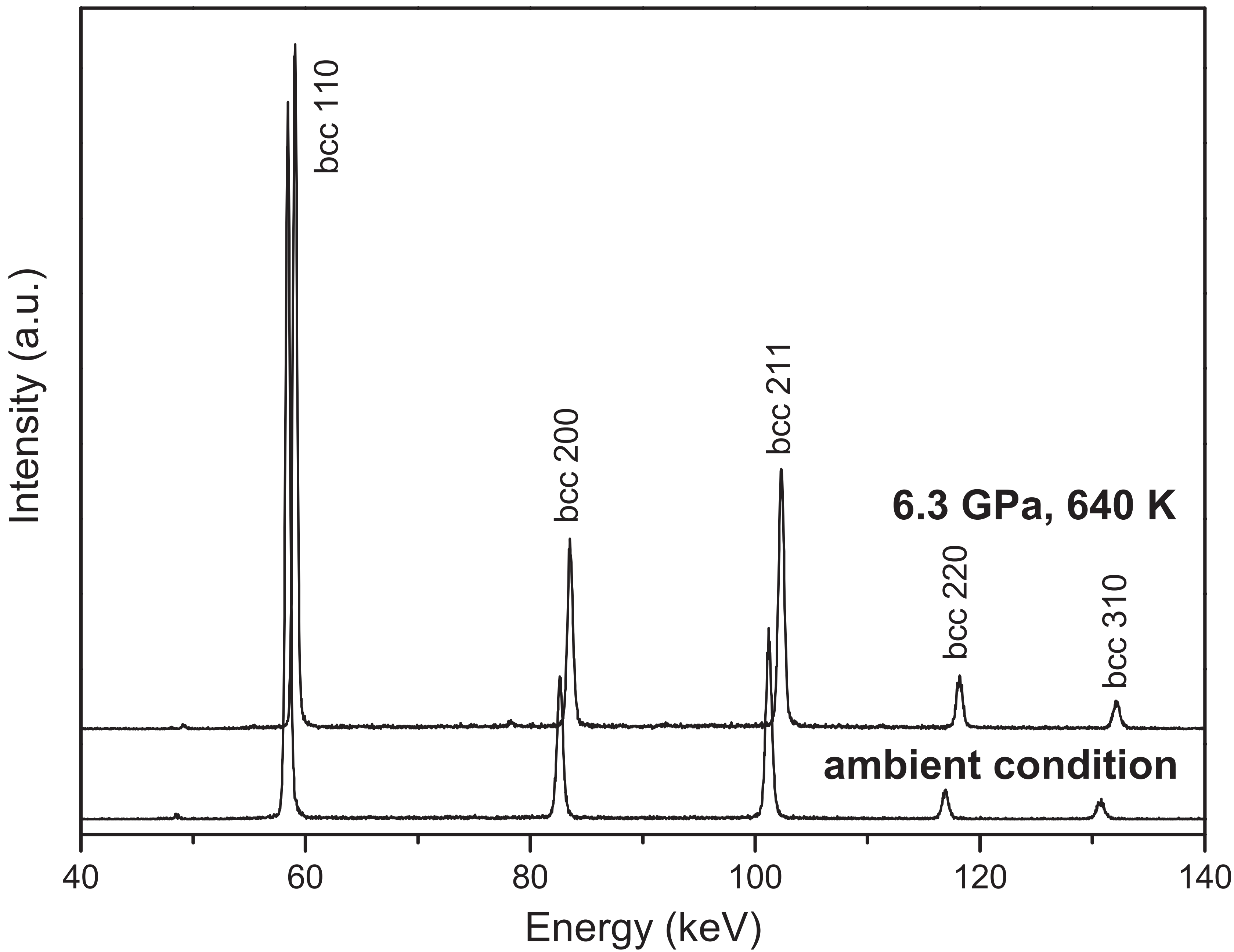

bcc 110
bcc 200
bcc 211
6.3 GPa, 640 K
bcc 220
bcc 310
ambient condition
Intensity (a.u.)
40
60
80
100
120
140
Energy (keV)

Figure 3 revised

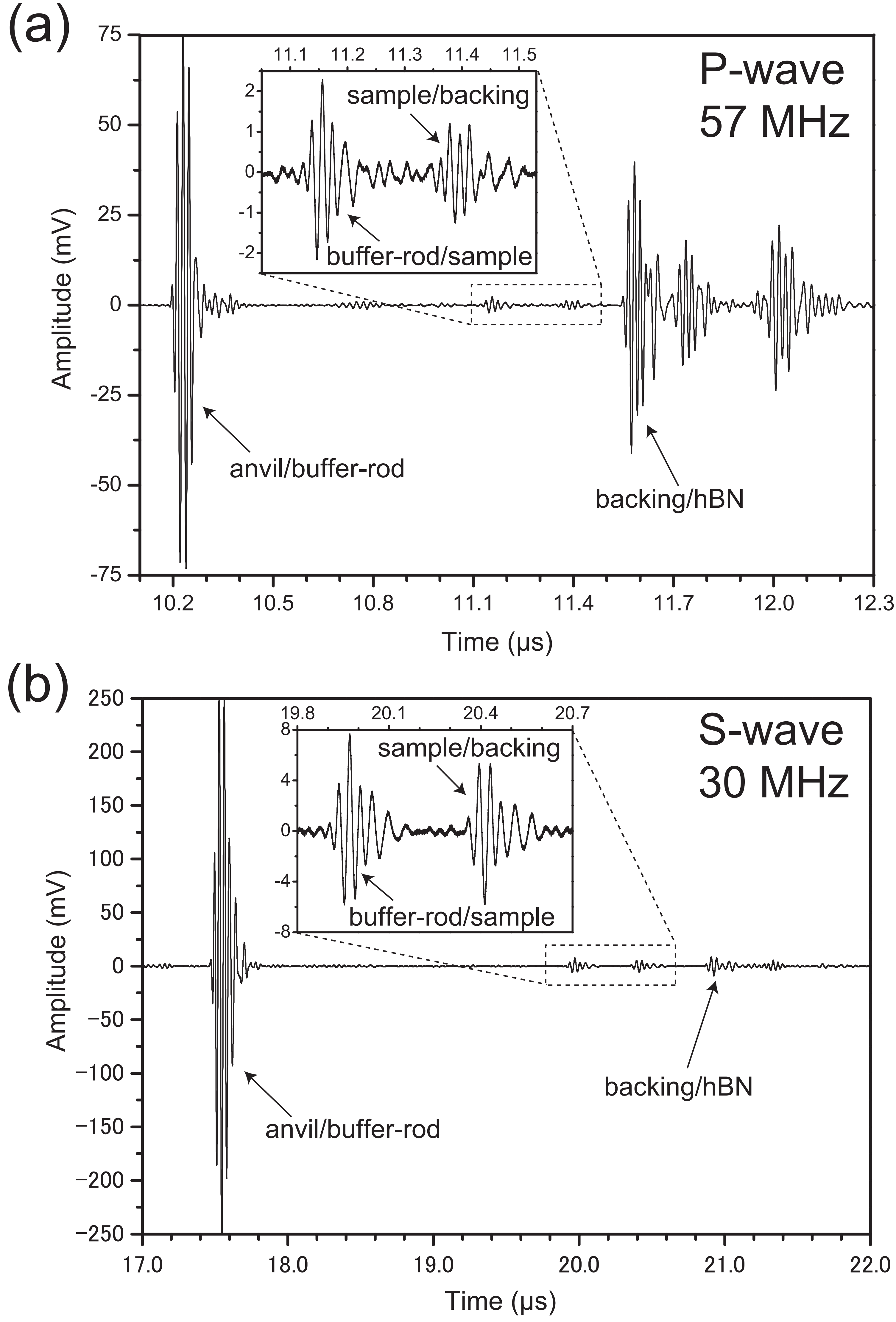

Figure 4

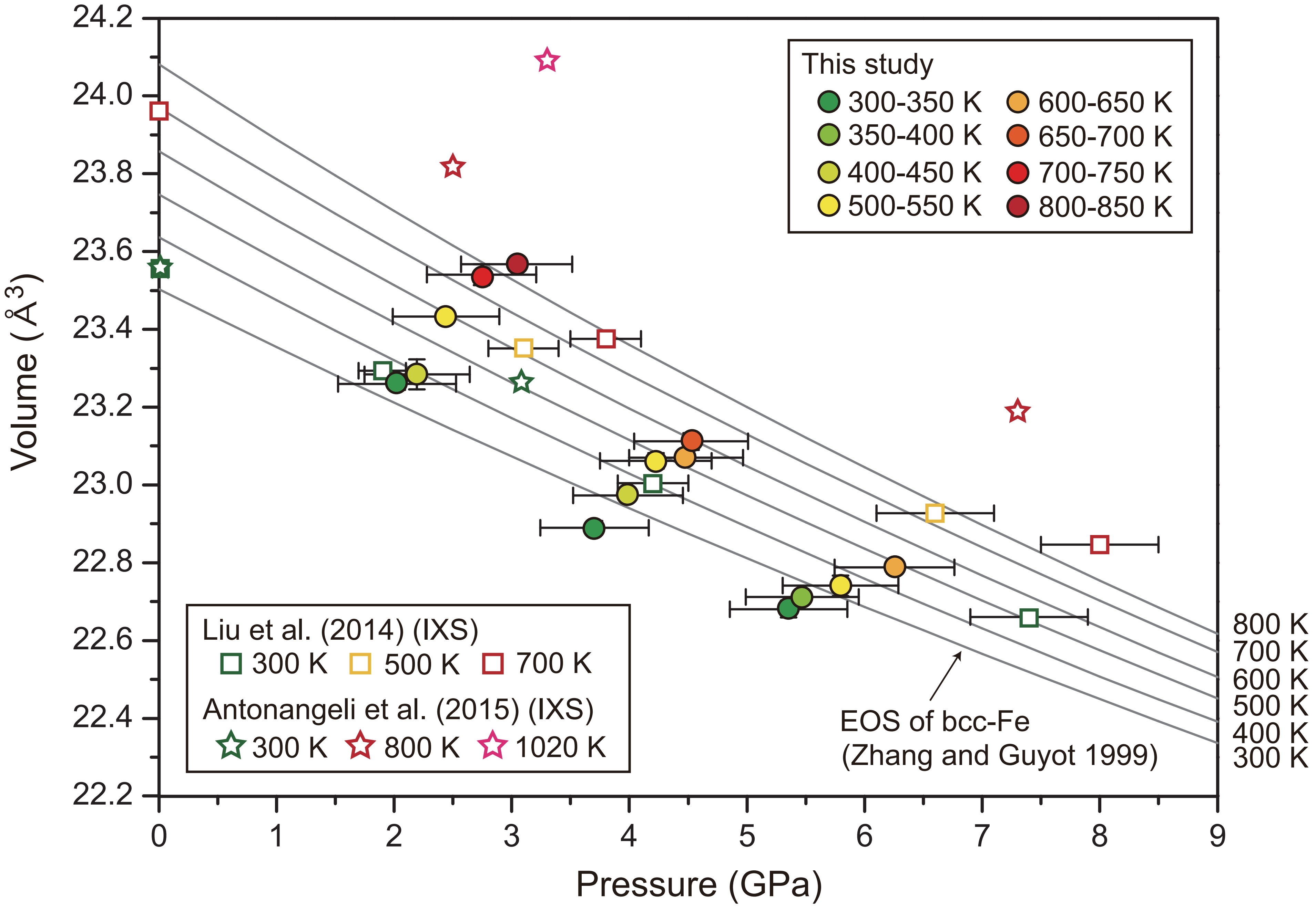

This study
300-350 K
350-400 K
400-450 K
500-550 K
600-650 K
650-700 K
700-750 K
800-850 K
Liu et al. (2014) (IXS)
300 K
500 K
700 K
Antonangeli et al. (2015) (IXS)
300 K
800 K
1020 K
EOS of bcc-Fe
(Zhang and Guyot 1999)
800 K
700 K
600 K
500 K
400 K
300 K
Volume (Å^3)
Pressure (GPa)
24.2
24.0
23.8
23.6
23.4
23.2
23.0
22.8
22.6
22.4
22.2
0
1
2
3
4
5
6
7
8
9

Figure 5 revised

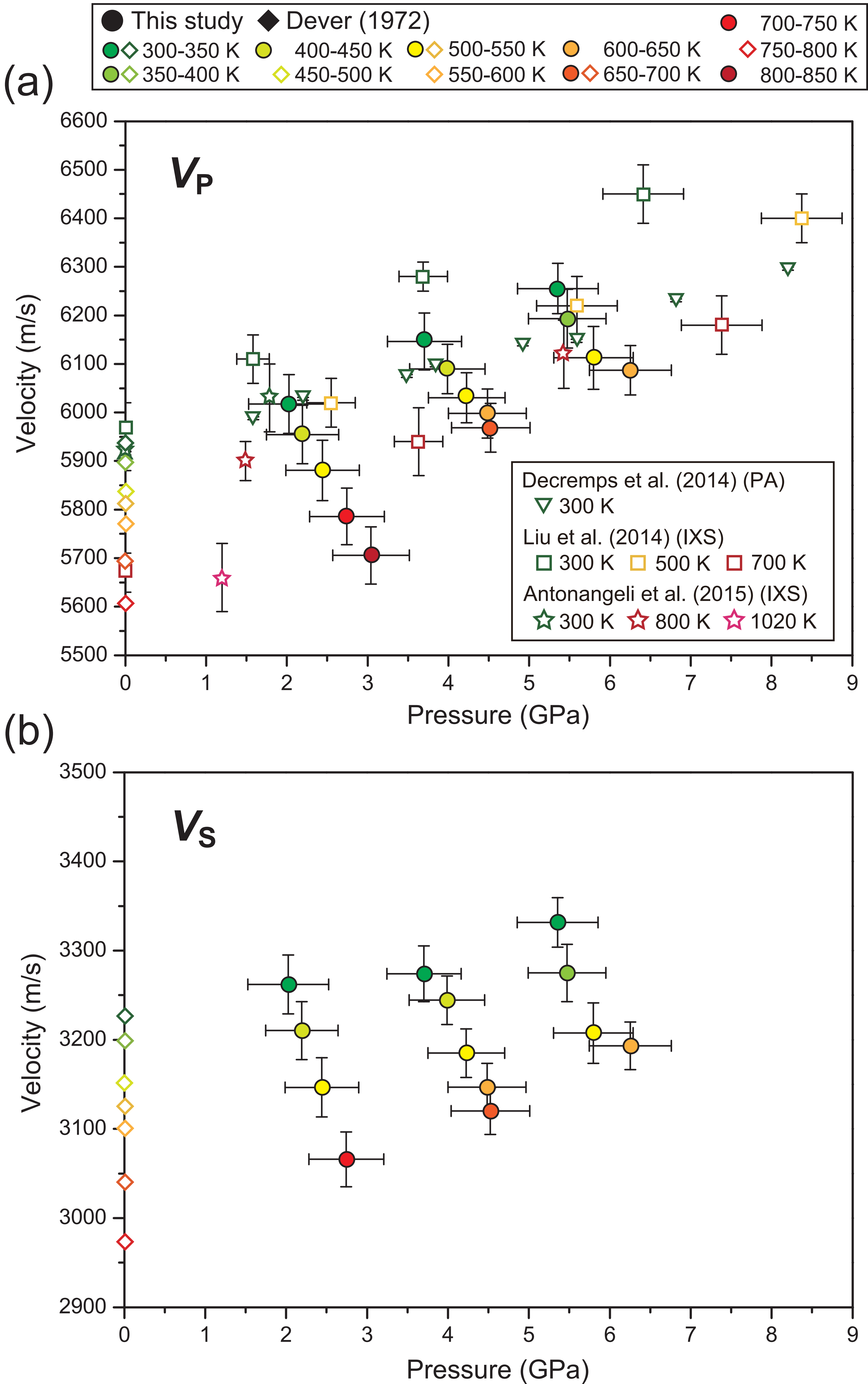

Figure 6

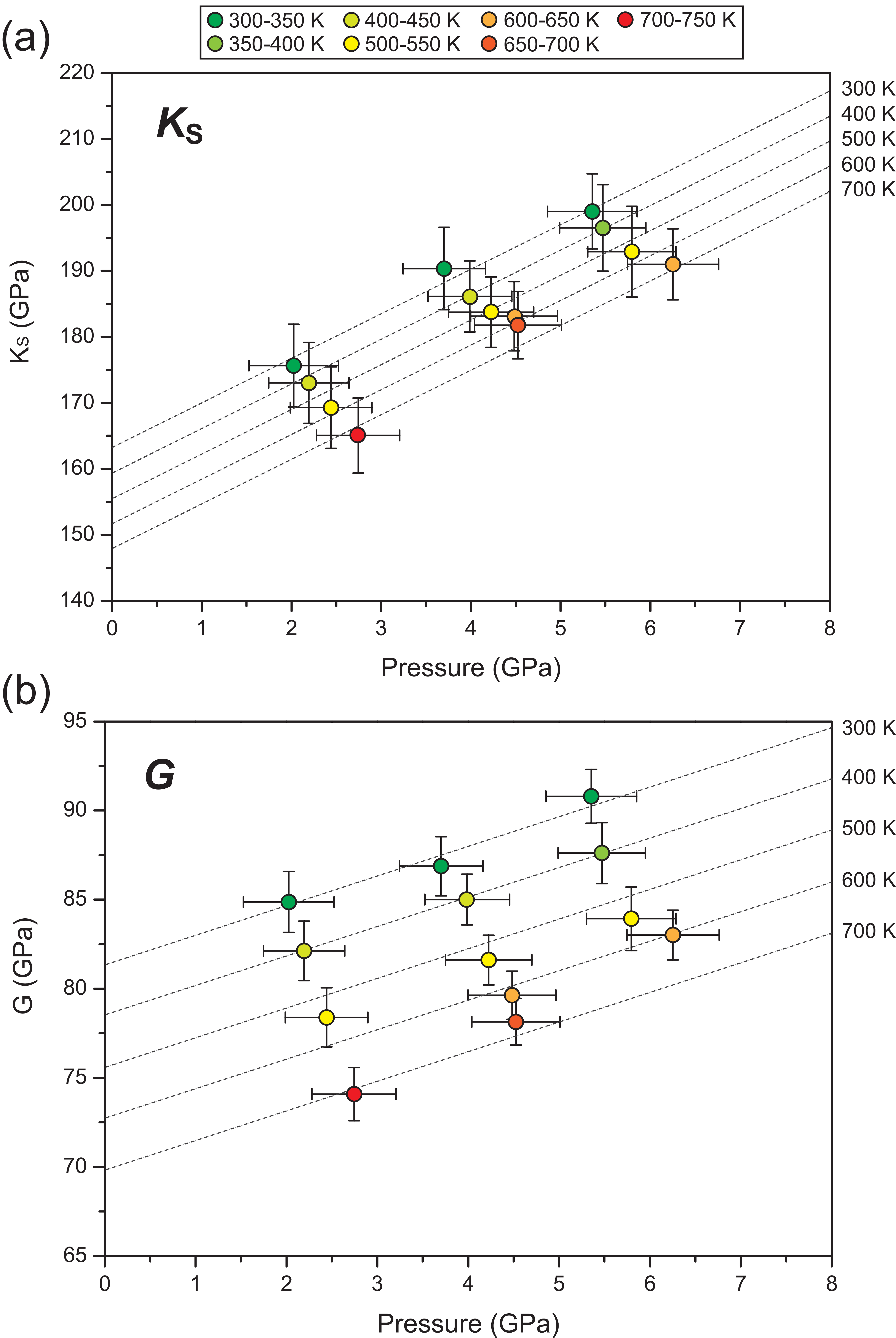

(a)
300-350 K
400-450 K
600-650 K
700-750 K
350-400 K
500-550 K
650-700 K
K_S
K_S (GPa)
Pressure (GPa)
300 K
400 K
500 K
600 K
700 K
(b)
G
G (GPa)
Pressure (GPa)
300 K
400 K
500 K
600 K
700 K

Figure 7

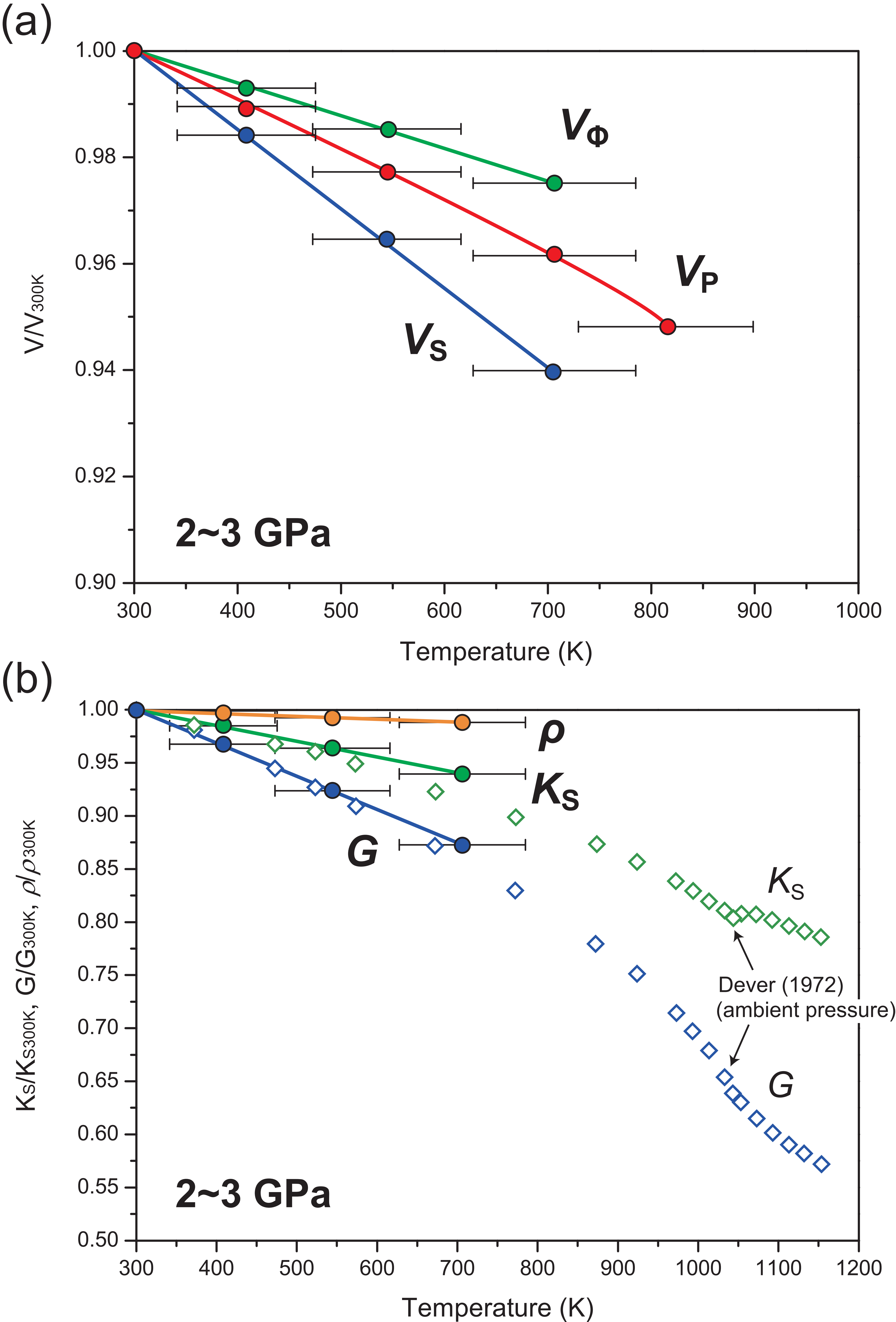
(a)
1.00
0.98
0.96
0.94
0.92
0.90
V/V300K
VΦ
VP
VS
2~3 GPa
300
400
500
600
700
800
900
1000
Temperature (K)
(b)
1.00
0.95
0.90
0.85
0.80
0.75
0.70
0.65
0.60
0.55
0.50
KS/KS300K, G/G300K, ρ/ρ300K
ρ
KS
G
KS
Dever (1972)
(ambient pressure)
G
2~3 GPa
300
400
500
600
700
800
900
1000
1100
1200
Temperature (K)

Figure 8 revised

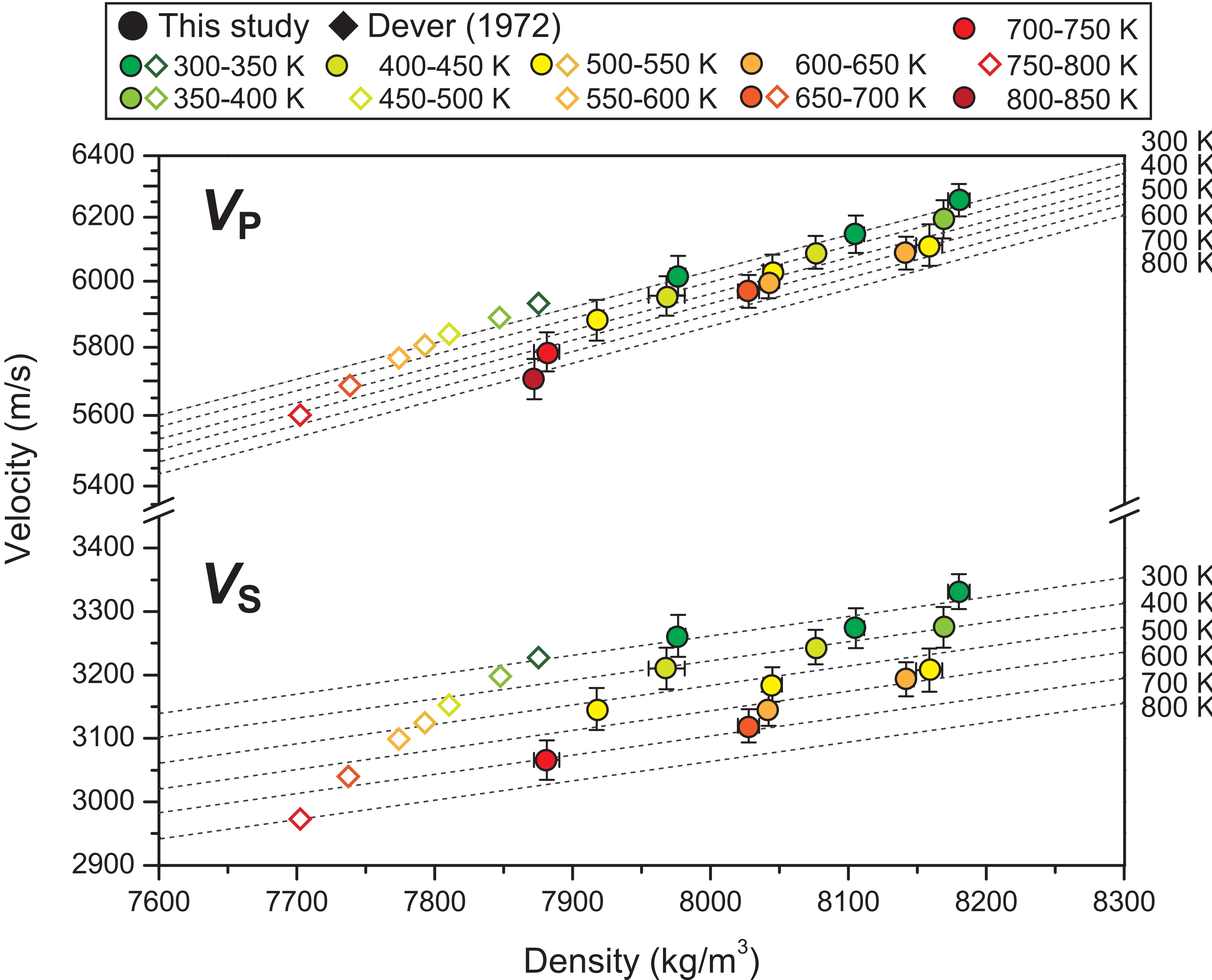

Figure 9 revised

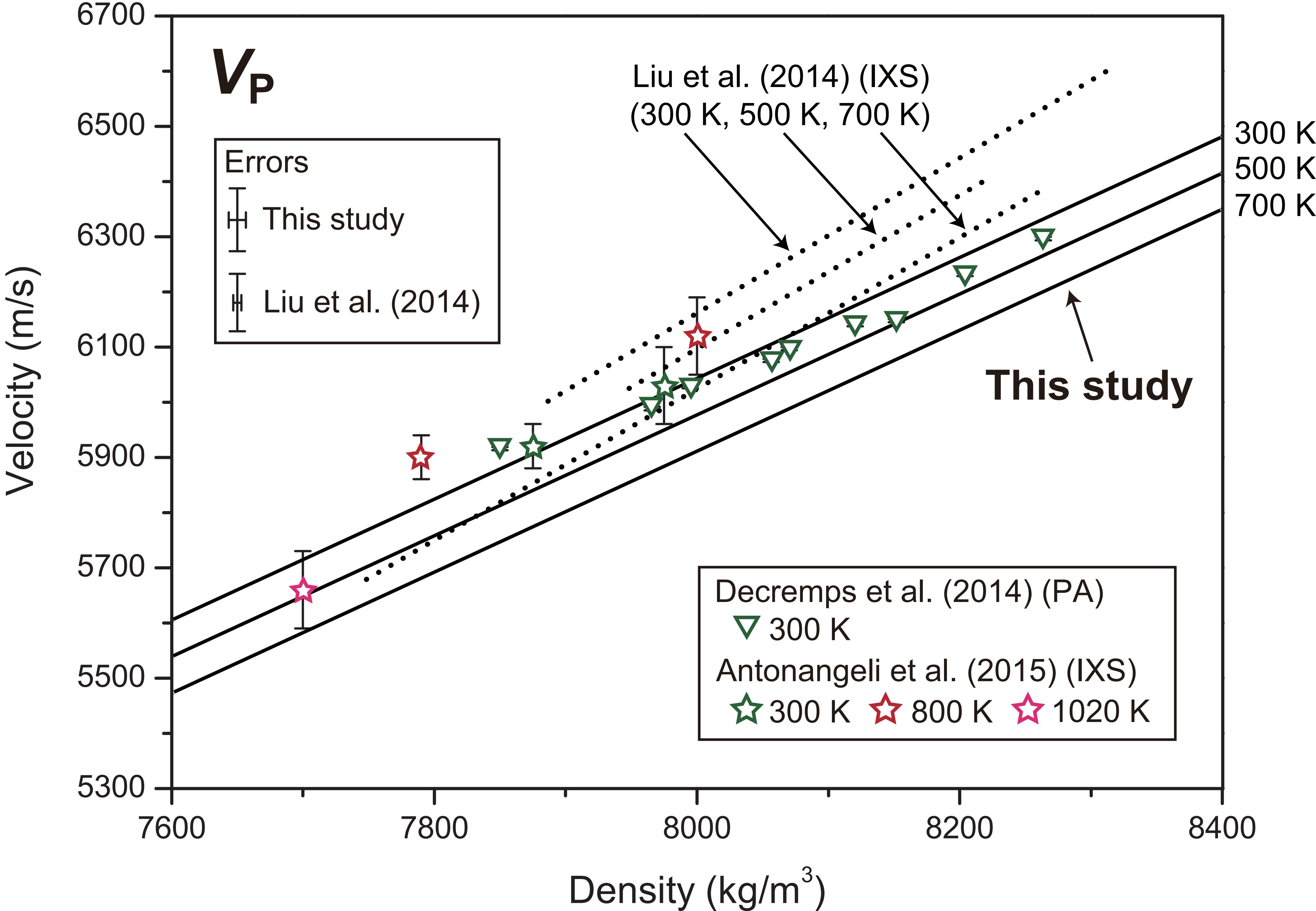

Figure 10

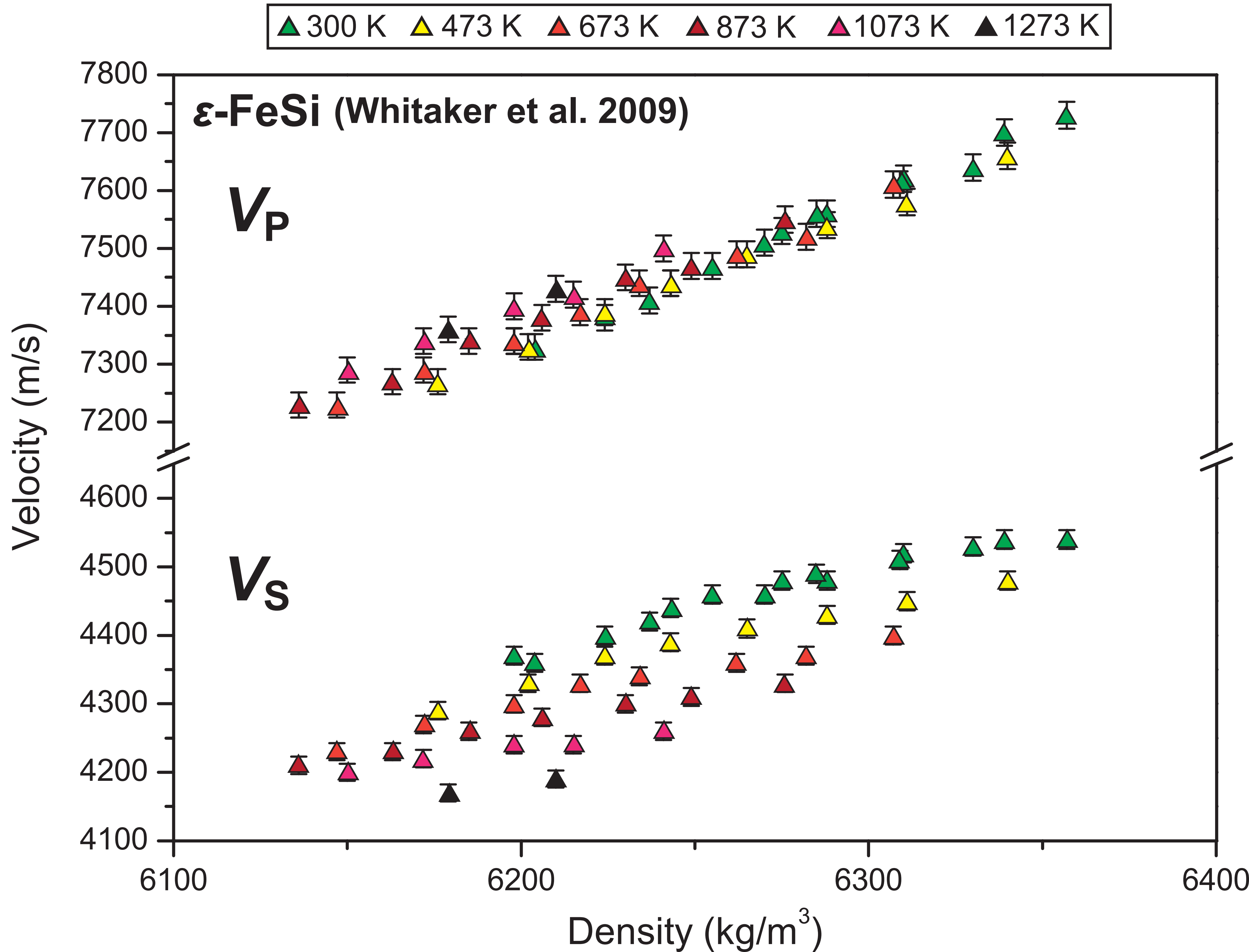

300 K
473 K
673 K
873 K
1073 K
1273 K
ε-FeSi (Whitaker et al. 2009)
V_P
V_S
Velocity (m/s)
Density (kg/m^3)
7800
7700
7600
7500
7400
7300
7200
4600
4500
4400
4300
4200
4100
6100
6200
6300
6400

Figure 11

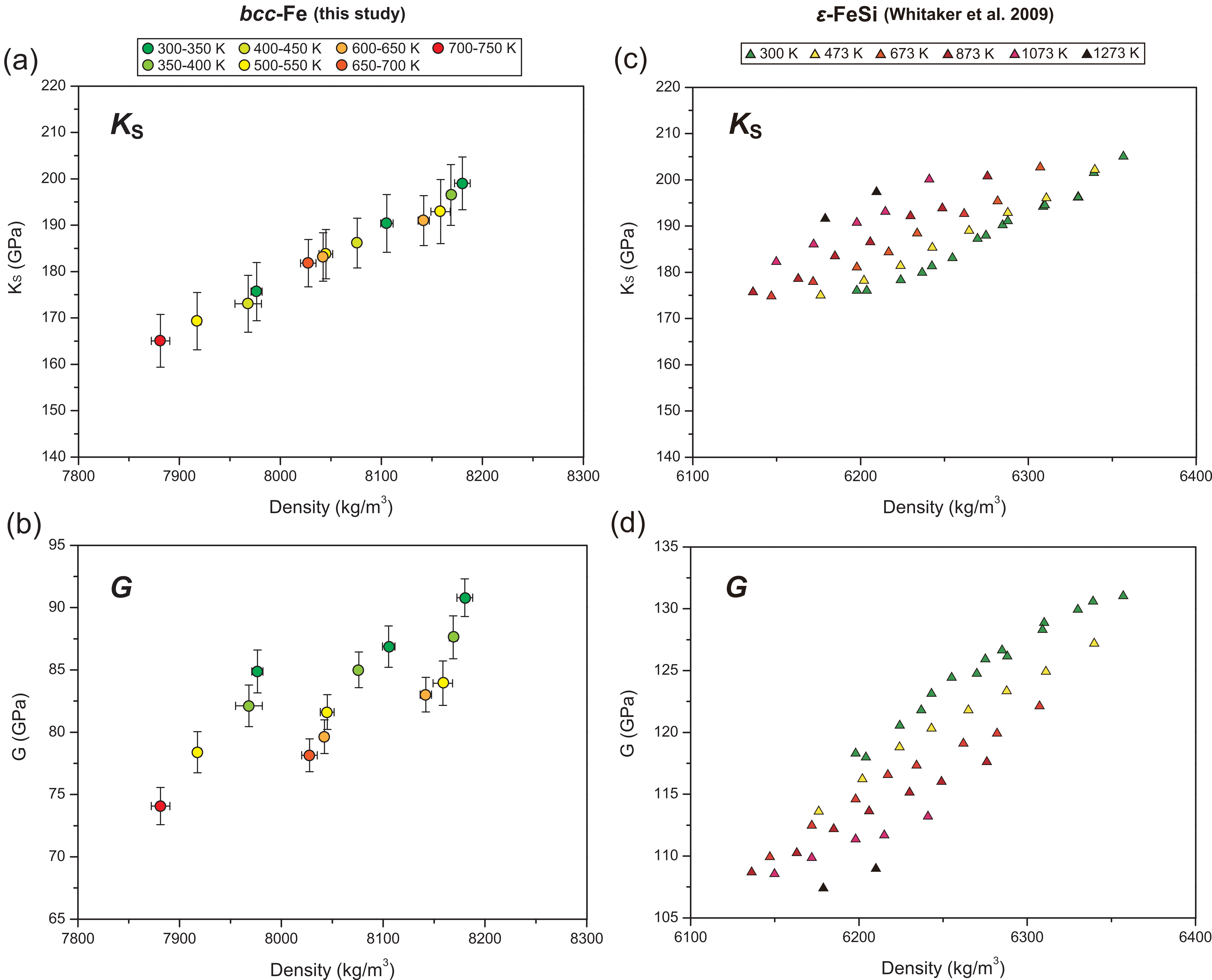

bcc-Fe (this study)
ε-FeSi (Whitaker et al. 2009)
300-350 K
400-450 K
600-650 K
700-750 K
350-400 K
500-550 K
650-700 K
300 K
473 K
673 K
873 K
1073 K
1273 K
(a)
(b)
(c)
(d)
K_S
G
K_S (GPa)
G (GPa)
Density (kg/m^3)